COMPARATIVE STUDY OF NANOTUBE AND NANOSHEET TiO_2 ON PHOTODEGRABILITY OF LDPE/TiO_2 FILMS

PRATYA KUNJIT

A THESIS SUBMITTED IN PARTIAL FULFILLMENT OF THE REQUIREMENT FOR THE DEGREE OF MASTER OF SCIENCE IN POLYMER TECHNOLOGY
DEPARTMENT OF CHEMISTRY FACULTY OF SCIENCE
KING MONGKUT'S INSTITUTE OF TECHNOLOGY LADKRABANG
2019

KMITL-2018-SC-M-014-074

COMPARATIVE STUDY OF NANOTUBE AND NANOSHEET TiO_2 ON PHOTODEGRABILITY OF LDPE/TiO_2 FILMS

PRATYA KUNJIT

A THESIS SUBMITTED IN PARTIAL FULFILLMENT OF THE REQUIREMENT FOR THE DEGREE OF MASTER OF SCIENCE IN POLYMER TECHNOLOGY

DEPARTMENT OF CHEMISTRY FACULTY OF SCIENCE
KING MONGKUT'S INSTITUTE OF TECHNOLOGY LADKRABANG

2019
KMITL-2018-SC-M-014-074

การศึกษาเชิงเปรียบเทียบของนาโนทิว และนาโนชีทของ TiO_2 ต่อการย่อยสลายด้วยแสงของฟิล์ม LDPE/TiO_2

COMPARATIVE STUDY OF NANOTUBE AND NANOSHEET TiO_2 ON PHOTODEGRABILITY OF LDPE/TiO_2 FILMS

ปรัชญา ขุนจิตต์

PRATYA KUNJIT

วิทยานิพนธ์นี้เป็นส่วนหนึ่งของการศึกษาตามหลักสูตร

ปริญญาวิทยาศาสตรมหาบัณฑิต สาขาวิชาเทคโนโลยีพอลิเมอร์

ภาควิชาเคมี คณะวิทยาศาสตร์

สถาบันเทคโนโลยีพระจอมเกล้าเจ้าคุณทหารลาดกระบัง

พ.ศ. 2562

KMITL-2018-SC-M-014-074

หัวข้อวิทยานิพนธ์	การศึกษาเชิงเปรียบเทียบของนาโนทิว และนาโนชีทของ TiO_2 ต่อการย่อยสลายด้วยแสงของฟิล์ม LDPE/ TiO_2
ชื่อนักศึกษา	นายปรัชญา ขุนจิตต์
รหัสประจำตัว	57605048
ปริญญา	วิทยาศาสตรมหาบัณฑิต (เทคโนโลยีพอลิเมอร์)
ภาควิชา	เคมี
พ.ศ.	2562
อาจารย์ที่ปรึกษาวิทยานิพนธ์	ผศ.ดร.ชลลดา ฤตวิรุฬห์
อาจารย์ที่ปรึกษาวิทยานิพนธ์ร่วม	ศ.ดร.ตะวัน สุขน้อย
	ผศ.ดร.สุภารัตน์ รักชลธี

บทคัดย่อ

งานวิจัยนี้ศึกษาฟิล์มพอลิเอทิลีนชนิดความหนาแน่นต่ำ (LDPE) ที่ย่อยสลายได้ด้วยแสงโดยใช้ตัวเร่งปฏิกิริยาไททาเนียมไดออกไซด์ (P25) ไททาเนตนาโนทิวบ์ (TNT) และ ไททาเนตนาโนชีท (TNS) สังเคราะห์ TNT โดยวิธีการไฮโดรเทอร์มอลและเผา ที่อุณหภูมิ 300, 400, 500 และ 600 องศาเซลเซียส สังเคราะห์เลพิโดโครไซต์ไททาเนตโดยวิธีโซลิดสเทตตามด้วยการทำโปรตอนเอ็กซ์เชนจ์ จากนั้นทำการเอกซ์โฟลิเอชันกับเตตระบิวทิลแอมโมเนียมไฮดรอกไซด์ (TBAOH) ให้ได้เป็น TNS/TBA^+ โดยศึกษาปัจจัยที่มีผลต่อการย่อยสลายของฟิล์ม LDPE ได้แก่ ชนิดของตัวเร่งปฏิกิริยาที่ 0.5 phr ของ P25, TNT(400) และ TNS/TBA^+ และปริมาณของตัวเร่งปฏิกิริยาที่ 0.5 และ 1.0 phr ของ P25 และ TNT(400) ทำการพิสูจน์เอกลักษณ์ของตัวเร่งปฏิกิริยาด้วยเทคนิคการเลี้ยวเบนรังสีเอกซ์ (XRD) เทคนิควิเคราะห์หาพื้นที่ผิวจำเพาะ (BET) กล้องจุลทรรศน์อิเล็กตรอนแบบส่องผ่าน (TEM) เทคนิคดิฟฟิวซ์รีเฟคแทนยูวีวิสิเบิลสเปกโทรมิเตอร์ (DR-UV-vis Spectrometer) และการย่อยสลายทางแสงของตัวเร่งปฏิกิริยาด้วยสารละลายเมทิลออเรนจ์ (MO) เตรียมคอมปาวด์โดยใช้เครื่องผสมระบบปิด และขึ้นรูปฟิล์มด้วยกระบวนการกดอัด ศึกษาการย่อยสลายทางแสงของฟิล์มภายใต้แสงยูวีเอ (UVA) ด้วยตู้ฉายแสง UVA เป็นเวลา 0, 50, 100, 150 และ 200 ชั่วโมง จากนั้นนำฟิล์มไปหาค่าดัชนีคาร์บอนิล (C.I.) ร้อยละน้ำหนักของฟิล์มที่หายไป การเปลี่ยนแปลงสีของฟิล์ม (ΔE) เปอร์เซ็นต์ความทึบแสง ศึกษาสัณฐานวิทยา และสมบัติเชิงกลของฟิล์ม สามารถเตรียมตัวเร่ง TNT และ TNS/TBA^+ ได้สำเร็จ พบว่า TNT และ TNS/TBA^+ มีพื้นที่ผิวจำเพาะสูงกว่า P25 เนื่องจากการเปลี่ยนแปลงโครงสร้างของตัวเร่งปฏิกิริยา นอกจากนั้นพบว่า P25 มีค่าช่องว่างแถบพลังงานต่ำที่สุด ส่งผลให้การสลายตัวของ MO สูงที่สุด เพราะ P25 มีวัฏภาคอนาเทสมากและมีวัฏภาคผสมของรูไทล์ เมื่อทำการผสมฟิล์มที่มี TNS/TBA^+ มีการกระจายตัวที่ดีกว่า P25 และ TNT(400) เนื่องจาก TBA^+ กับ

LDPE ไม่มีขั้วเหมือนกัน หลังการฉายแสง UVA ฟิล์มมีค่าดัชนีคาร์บอนิล (C.I.) เปอร์เซ็นต์น้ำหนักที่หายไป ค่าการเปลี่ยนแปลงสี (ΔE) และค่าการเปลี่ยนแปลงความสว่าง (ΔL) เพิ่มขึ้น เปอร์เซ็นต์ความทึบแสงของฟิล์มที่มี TNS/TBA^+ มีค่าน้อยกว่าฟิล์มที่มี P25 หรือ TNT(400) เนื่องจากฟิล์มที่มี TNS/TBA^+ มีการกระจายตัวที่ดี ทำให้แสงสามารถส่องผ่านและเกิดการกระเจิงแสงในฟิล์มได้น้อย ค่าความแข็งแรงดึง ณ จุดขาด และมอดุลัสของยังเพิ่มขึ้นเล็กน้อย ขณะที่เปอร์เซ็นต์การดึงยืด ณ จุดขาดมีค่าลดลง เนื่องจากการสลายตัวของฟิล์ม การเพิ่มปริมาณตัวเร่งช่วยเพิ่มการย่อยสลายทางแสง เนื่องจากตัวเร่งสามารถดูดกลืนแสง UVA ทำให้เกิดโมเลกุลที่มีความว่องไวได้มากขึ้น เช่น •OH, O_2•- and HO_2• ซึ่งช่วยเพิ่มประสิทธิภาพในการย่อยสลายฟิล์ม

คำสำคัญ : การย่อยสลายได้ด้วยแสง, ไททาเนตนาโนชีท, ไททาเนตนาโนทิว, ไททาเนียมไดออกไซด์, พอลิเอทิลีนชนิดความหนาแน่นต่ำ

Thesis Title	Comparative study of nanotube and nanosheet TiO_2 on photodegrability of LDPE/TiO_2 films
Student Name	Mr. Pratya Kunjit
Student ID	57605048
Degree	Master of Science (Polymer Technology)
Department	Chemistry
Year	2019
Thesis Advisor	Asst. Prof. Dr. Chonlada Ritvirulh
Thesis Co-advisors	Prof. Dr. Tawan Sooknoi
	Asst. Prof. Dr. Suparat Rukchonlatee

Abstract

This research studied on photocatalytic degradation of low-density polyethylene (LDPE) films incorporated with titanium dioxide (TiO_2) as P25, titanate nanotube (TNT) and titanium nanosheet (TNS). TNT was synthesized from hydrothermal method and calcined for 2 hours at 300, 400, 500 and 600°C. Lepidocrocite titanate was obtained from a solid-state synthesis, followed by proton exchange then exfoliation of tetrabutylammonium hydroxide (TBAOH) into TNS/TBA^+. The effect of catalyst types at 0.5 phr of P25, TNT(400) and TNS/TBA^+ were observed. The effect of catalyst loading at 0.5 and 1.0 phr of P25 and TNT(400) on degradation of the photodegradable LDPE films were investigated. The catalysts were characterized using X-ray diffractometer (XRD), Brunauer–Emmett–Teller surface area analyzer (BET), transmission electron microscope (TEM), diffuse reflectance UV-visible spectrometer (DR-UV-vis) and photocatalytic degradation of methyl orange (MO) of catalysts. Compounds were prepared using an internal mixer then shaped with a compression molding process. Photodegradable films were placed in UVA box for 0, 50, 100, 150 and 200 hours to study photodegradation. In addition, carbonyl index (C.I.), %weight loss, color change (ΔE), %opacity, morphology and mechanical properties of the films were examined. TNT and TNS/TBA^+ was successfully prepared. TNT and TNS/TBA^+ had a higher surface area than P25 owing to structure change. Moreover, P25 exhibited the lowest band gap energy, leading to the highest degradation of MO. This is because P25 had high

intensity of anatase phase including mixed phases of rutile. LDPE mixed with TNS/TBA^+ revealed a better dispersion than LDPE mixed with P25 or TNT(400) due to non-polarity of TBA^+ and LDPE. Photodegradation of the films after UVA exposures were increased in carbonyl index (C.I.), %weight lost, color change (**Δ**E) and lightness change (**Δ**L). %Opacity of LDPE mixed with TNS/TBA^+ was better than LDPE mixed with P25 or TNT(400) because of good dispersion in LDPE. It is suggested that, TNS/TBA^+ allowed light to transmit and low light scattering in LDPE film was occurred. Photodegradable films after UVA exposures were slightly increased in tensile strength at break and Young's modulus. While %elongation at break was decreased owing to the degradation of the film. An increment of catalyst loading improved photocatalytic degradation. This is because catalyst could absorb more UVA light, resulting in the larger amount of several active oxygen species such as •OH, O_2•- and HO_2• that enhanced the ability of film degradation.

Keywords : Photocatalytic degradation, Titanium nanosheet (TNS), Titanate nanotube (TNT), Titanium dioxide (TiO_2), Low-density polyethylene (LDPE)

Acknowledgements

The author would like to express our sincere appreciation to the project advisor and co-advisor Asst. Prof. Dr. Chonlada Ritvirulh, Prof. Dr. Tawan Sooknoi and Asst. Prof. Dr. Suparat Rukchonlatee for their supports, supervision, inspiration, suggestion and encouragement throughout this thesis.

I would like to thank Prof. Dr. Suwabun Chirachanchai, Assoc. Prof. Dr. Ittipol Jangchud and Dr. Tosapol Maluangnont for serving as the chairperson and the committee and for valuable comments.

I would also appreciate the supports from the Department of Chemistry, Faculty of Science, King Mongkut's Institute of Technology Ladkrabang for the equipment, chemicals and facilities.

I would like to extend our sincere appreciation to all teachers, supporting staff and friends for their constant guidance, advice, support and encouragement.

Finally, I deeply appreciate and thank our parents and family for their love and supports.

Mr. Pratya Kunjit

Table of Contents

Table of Contents (Continued)

Table of Contents (Continued)

List of Tables

List of Figures

List of Figures (Continued)

Figure **Page**

Chapter 1
Introduction

1.1 Research motivation

Plastic becomes one of the most widely used materials for several applications, such as packaging, electrical equipment, household equipment and vehicles etc. Polyethylene is a popular polymer due to its low melting temperature, easy to process, excellent chemical resistance and low cost. Especially, low density polyethylene (LDPE) that has high tensile and impact strength, is used in packaging. However, plastic waste has a negative impact to environment. It is usually non-biodegradable and therefore can remain as waste for a very long time. For example, LDPE has been estimated to break down within an average time of 1000 years [1]. Plastic may risk to human health as well as the environment and it is somewhat difficult to reuse and/or recycle. To reduce plastic waste problem, the development of plastic that can be easily degraded is interesting.

There are many kinds of degradable plastic. Mechanical degradation is a common process to break down plastic into small pieces but waste is remained. Oxidative degradation involves plastics with functional group, such as hydroxyl group (-OH) and carbonyl group (-C=O), which absorb light and break some of the C-C bonds. Hydrolytic degradation can be used for polymer with ester or amide group that can be broken down by hydrolysis. Biodegradable plastic can be attacked by bacteria, fungi or other micro-organisms. However, LDPE does not possess –OH, -C=O and ketone functional groups, which cannot be degraded by oxidative degradation, hydrolytic degradation and biodegradation. While photodegradation uses UV-Visible light to activate electron in catalyst that can attack the C-C bond of LDPE [2]. Hence, photocatalysis may well be applied for LDPE degradation. This is because photocatalytic degradation can be accomplished simply by leaving plastic filled with photocatalysts on the ground. The waste plastic will be gradually degraded into soil by sunlight.

Among all photocatalysts, titanium dioxide (TiO_2) is considered to be very competitive due to its nontoxic nature, low cost, high reactivity and renewable material. However, the compatibility of TiO_2 with plastic especially LDPE is poor giving films with defects and impaired mechanical properties. The poor compatibility of TiO_2

with LDPE leads to agglomeration of TiO_2 particles that light could not pass through film relating in film opacity. This is not satatistory for use as some packaging that require transparency. To improve optical properties of the photodegradable film, nanostructure material is of interest. In addition to typical TiO_2, i.e. anatase and rutile, titanate nanostructure materials such as nanotubes, nanofibers and nanosheets have also attracted attention for their use in photocatalysis [3]. Compared to spherical particles of TiO_2, the titanate nanotube and nanosheet could provide relatively high surface area. This can improve compatibility with LDPE, enhance film transparency, reduce defects and also increase mechanical strength of the films. The catalyst also enhances interfacial charge transfer rate that reduces the electron/hole (e^-/h^+) recombination probability, and hence facilitates photodegradation ability [4] with low opacity.

In this work, different titanate nanostructures (i.e. nanotube and nanosheet) as photocatalyst materials were prepared, and mixed with LDPE. The photodegradable LDPE films with titanate nanostructures were tested for photodegradation activity, mechanical properties and optical properties as compared to the LDPE film with typical TiO_2.

1.2 Objectives of the study

To compare LDPE mixed with differences titanate nanostructures and catalysts loading on band gap energy, physical and mechanical properties of the photodegradable films.

1.3 Scopes of the study

1. Synthesis of titanate nanotube from hydrothermal method and lepidocrocite titanate from solid state synthesis.

2. Exfoliation of lepidocrocite titanate into titanate nanosheet.

3. Characterization of titanate nanotube, lepidocrocite titanate and titanate nanosheet using X-ray diffraction (XRD), Brunauer–Emmett–Teller surface area analysis (BET), thermogravimetric analysis (TGA), transmission electron microscopy (TEM) and diffuse reflectance UV-visible spectrometry (DR-UV-vis).

4. Testing on photocatalytic oxidation of methyl orange (MO) over P25 (Typical TiO_2), titanate nanotube and titanate nanosheet under UV light for 0-30 minutes.

5. Mixing LDPE with P25, titanate nanotube and titanate nanosheet at various loadings of 0.5-1.0 phr.

6. Characterization of photodegradable LDPE films on tensile properties using universal testing machine, thermal property using differential scanning calorimetry (DSC), and morphology using scanning electron microscopy (SEM).

7. Study on photodegradation activity of photodegradable LDPE films by exposure under UV light for 200 hours.

8. Characterization of degraded photodegradable LDPE films on carbonyl index, %weight loss, color change, lightness change, %opacity and tensile properties.

1.4 Benefits of the study

It is expected that better optical properties of photodegradable LDPE film can be obtained, which assists in the development of photodegradable film and hence reduces plastics waste problem and global warming in the future.

Chapter 2
Theory and Literature Reviews

2.1 Degradable plastics [5-6]

Degradable plastics are designed to degrade in different ways and in different environments. The impacts of degradable plastics at end-of-life depend on the characteristics of the polymer itself (i.e. what the polymer is made from and how it is designed to degrade), the thickness and surface area of the product, as well as the disposal environment. There are insufficient data to say with any certainty, how long many degradable plastics take to fully degrade, and the impacts of any end products in the environment. Plastics can degrade in a number of different ways. There are four different types of degradable polymers.

1. Oxo-biodegradable plastics

Oxo-biodegradable plastics are those that undergo controlled degradation through the incorporation of prodegradant additives that can trigger and accelerate the degradation process. The oxidative degradation of these polymers can be accelerated by initiation of natural daylight, heat and/or mechanical stress and embrittle in the environment and erode under the influence of weathering.

2. Water-soluble plastics

Water-soluble plastics dissolve in water within a designated temperature range and then biodegrade in contact with microorganisms.

3. Biodegradable plastics

Biodegradable plastics are those that are capable of undergoing decomposition into carbon dioxide, methane, water, inorganic compounds or biomass in which the predominant mechanism is the enzymatic action of microorganisms that can be measured by standardized tests in a specific time, reflecting available disposal conditions.

4. Photodegradable plastics

Photodegradable plastics possess chain cleavage through the action of ultraviolet (UV) light, which degrades the chemical bond or link in the polymer or chemical structure of the plastics. This process can be assisted by the presence of UV-sensitive catalyst in the polymer.

2.2 Photodegradable plastics [7-9]

A degradable plastic in which the degradation results from the action of natural daylight is called a photodegradable plastic. The photo-induced degradation process can be initiated either by the absorption of the photon by the polymer chain itself or by some of the additives incorporated in the product. The degraded sites act as stress concentrators or crosslink of polymer chains. Thus, they change the tensile properties and cause the mechanical failure of the material.

The direct effect of radiation on plastic is usually limited to the surface region due to light absorption by the catalyst or the degraded material itself. Most of the synthetic polymers are susceptible to degradation initiated by UV and visible light. Normally the near-UV radiations (290-400 nm) in the sunlight determine the lifetime of polymeric materials in outdoor applications. Polymer degradation mainly occurs at the polar groups, where photo-irradiation generates ester, aldehyde and formate end groups. Photodegradation changes the physical and optical properties of the plastics. The most damaging effects are the visual effect (Yellowing), the change in mechanical properties, molecular weight and the molecular weight distribution of the polymers. In the case of photoactive catalyst like TiO_2, ZnO or CdS, formation of an electron-hole pair on the catalyst surface in the presence of oxygen and water can produce reactive species, which can eventually cause oxidation of the polymer.

2.3 Photodegradation

2.3.1 Catalysts [10-11]

Catalysts are capable of accelerating the reaction rate or changing the selectivity of the reaction towards different products with respect to the situation when the reaction occurs in absence of the catalyst.

Catalysts can be divided into two main types; homogeneous and heterogeneous.

1. Homogeneous catalysis

In a homogeneous reaction, the catalyst is in the same phase as the reactants. Typically, they can be presented as a gas or contained in a single liquid phase. A great variety of homogeneous catalysts are known, ranging from Bronsted and Lewis acids widely used in organic synthesis, metal complexes, metal ion, organometallic complexes, organic molecules and biocatalysts (Enzymes, artificial enzymes, etc.).

2. Heterogeneous catalysis

In a heterogeneous reaction, this involves the use of a catalyst in a different phase from the reactants. A typical example is a solid catalyst with the reactants in a separated phase. Most examples of heterogeneous catalysis undergo through the same stages:

- One or more of the reactants are adsorbed on to the surface of the catalyst at active sites.
- There are some sorts of interaction between the surface of the catalyst and the reactant molecules which makes them more reactive.
- The reaction occurs.
- The product molecules are desorbed.

A good catalyst needs to be adsorbed on the reactant molecules strongly enough for them to generate reaction, but not so strongly. The product molecules should be attached more or less permanently to the surface.

2.3.2 Mechanism of photodegradation [8, 12-13]

In photo-oxidative degradation (Equations 2.1-2.7), initially short-lived singlet state is transformed to long-lived triplet state. Catalyst absorbs UV light and generates mobile electrons and holes in the conduction and valence bands, respectively. Subsequent reactions with O_2 lead to the formation of several active oxygen species such as $^{\bullet}OH$, $O_2^{\bullet-}$, and $HO_2^{\bullet}$, of which $^{\bullet}OH$ is the most important oxidant in photocatalytic oxidation. The active oxygen species described above initiate the degradation reaction by attacking neighboring polymer chains and form radical pairs (Norrish type I reaction) or form pairs of saturated and unsaturated chain ends by hydrogen transfer (Norrish type II reaction). These, in turn, abstract hydrogen and form hydroperoxide groups, which absorb UV light or become excited by energy transfer. The weak O-O bonds break and pairs of alkoxy and hydroxyl radicals are formed, which may react in various ways, e.g. by hydrogen abstraction, chain scission, rearrangement, etc. and accelerate photodegradation. In photo-oxidative degradation, the mechanism involves an auto-oxidation cycle comprising of various steps as shown in Figure 2.1.

$TiO_2 + h\nu \longrightarrow TiO_2 (e^- + h^+)$ (2.1)

$O_2 + e\text{-} \longrightarrow O_2^{\bullet-}$ (2.2)

$O_2^{\bullet-} + H_2O \longrightarrow HO_2^{\bullet} + OH^-$ (2.3)

$2HO_2^{\bullet} \longrightarrow H_2O_2 + O_2$ (2.4)

$H_2O_2 + h\nu \longrightarrow 2^{\bullet}OH$ (2.5)

$OH^- + h^+ \longrightarrow {}^{\bullet}OH$ (2.6)

$H_2O + h^+ \longrightarrow {}^{\bullet}OH + H^+$ (2.7)

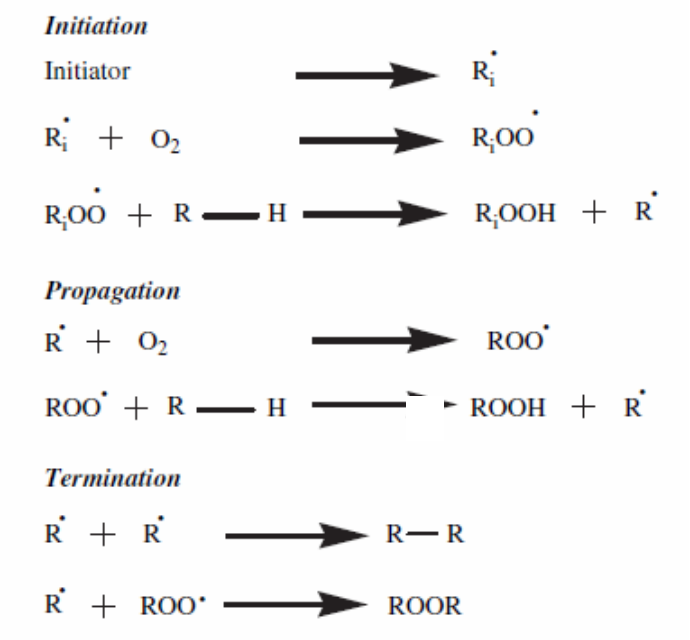

Figure 2.1 Photo-oxidative degradation on polymer chain [8]

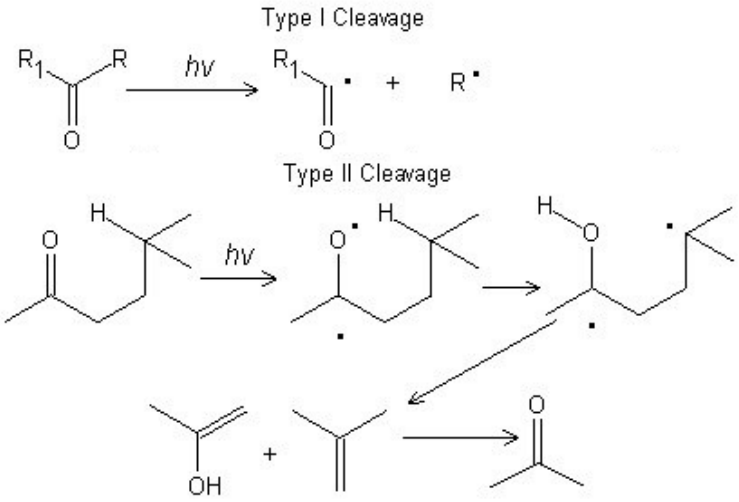

Figure 2.2 Norrish type I and type II reactions [14]

1. Initiation

Different initiation steps under various conditions have been noticed in different polymers. Photocatalysts are highly photosensitive and can be excited under an exposure to light. Catalyst residues are source of generation of radicals. The primary process involves the promotion of the electron to the conduction band of the semiconductor to form an electron-hole pair. The relative proportions of the reactive species depend on the presence of water. No catalyst sensitization will be observed unless both oxygen and water are present. Carbonyl groups formed by mild oxidation of polymer during processing act as chromophores and become source of the initiation radicals. Carbonyl absorbs near-UV radiations and subsequently forms radicals following Norrish type I, Norrish type II (Figure 2.2) and H-atom abstraction processes.

2. Propagation reaction

The propagating reactions of auto-oxidation cycle are common to all carbon backbone polymers. These reactions can lead to generation of hydroperoxide species that are intermediates to further reactions. Hydroperoxide species generated in propagating step could lead to backbone degradation through cleavage of hydroperoxide O-O bond followed by chain scission. The scission process generates two chain ends that are free to restructure and can often lead to an increase in crystallinity as oxidative degradation proceeds.

3. Termination reaction

This occurs naturally by combining free radicals or assists by stabilizers in the plastics. Peroxide radicals eventually terminate by reaction with other radicals to give di-alkyl peroxides, carbonyl species or alcohols.

2.4 Titanium dioxide [15-18]

Titanium dioxide (TiO_2) belongs to the family of transition metal oxides. In the beginning of the 20^{th} century, industrial production started with TiO_2 replacing toxic lead oxides as pigments for white paint. It is used as a white pigment in paints, plastic and paper, which represents the major end-use sectors of TiO_2. TiO_2 may be manufactured by either the sulfate or the chlorine processes. In the sulfate process, ilmenite is transformed into iron^{-} and titanium sulfates by reaction with sulfuric acid. Titanium hydroxide is precipitated by hydrolysis, filtered, and calcined at 900°C. This sulfate process yields a substantial amount of iron sulfides waste and a poor quality

TiO_2, although nowadays, the quality has improved significantly. Therefore, the chlorine process has now become the dominant method. The process involves a high temperature furnace to heat the ilmenite with coal and sulfur. The slurry of reduced ilmenite, consisting of a mixture of iron and TiO_2 in water, is oxidized with air and can be separated in settling ponds. The iron oxide is returned to the mine site as waste and for land filling process. The rutile is reacted with chlorine to produce titanium tetrachloride, which is purified and reoxidized, yielding very pure TiO_2.

TiO_2 has received a great deal of attention due to its chemical stability, non-toxicity, low cost and other advantageous properties. As a result of its high refractive index, it is used as anti-reflection coating in silicon solar cells and in many thin-film optical devices. TiO_2 is used as a biomaterial (e.g., bone substituent and reinforcing mechanical supports). TiO_2 is also used in catalytic reactions acting as a promoter, a carrier for metals and metal oxides, an additive, or as a catalyst.

Three polymorphs of TiO_2 (Figure 2.3) found in nature i.e., anatase (Tetragonal), rutile (Tetragonal) and brookite (Orthorhombic). Particle size experiments affirm that the relative phase stability may reverse when particle sizes decrease to sufficiently low values due to surface-energy effects (surface free energy and surface stress, which depend on particle size). If the particle sizes of the three crystalline phases are equal, anatase is most thermodynamically stable at sizes less than 11 nm, brookite is most stable between 11 and 35 nm, and rutile is most stable at sizes greater than 35 nm.

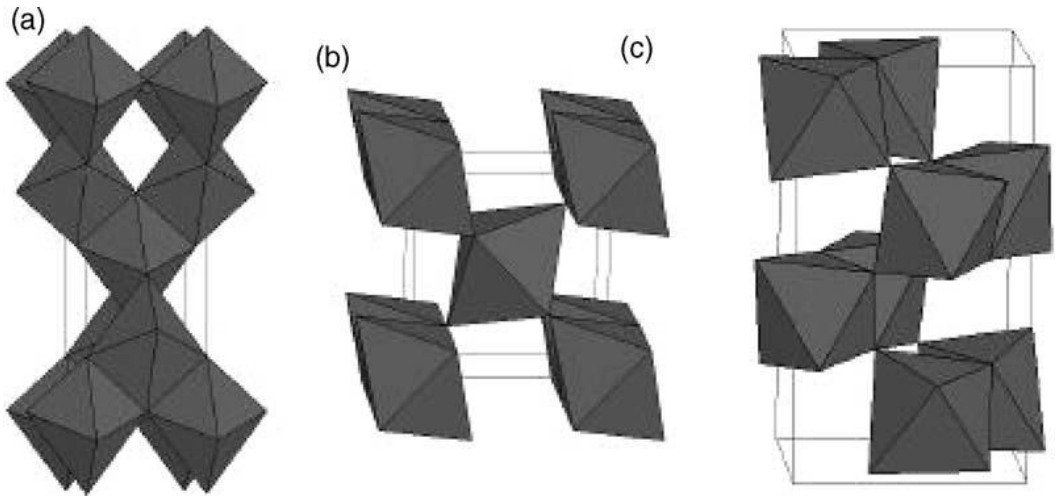

Figure 2.3 Crystal structures of anatase (a), rutile (b) and brookite (c) [16]

2.4.1 Degussa P25 [19-20]

Degussa P25 (Aeroxide TiO_2 P25) is a titanium photocatalyst that is used widely because of its relatively high levels of activity in many photocatalytic reaction systems. It is well known that P25 is composed of anatase and rutile crystallites, the reported ratio being typically 70:30 or 80:20. P25 with the co-presence of anatase and rutile crystallites induces the high level of photocatalytic activity that transfers of excited electrons and positive holes between interconnecting anatase and rutile particles may enhance charge separation and hence improve the efficiency of utilization of electron-hole pairs.

Applications

- Raw material for catalyst substrates with high thermal and hydrothermal stabilities
- Efficient catalyst substrate with good thermal and hydrothermal stabilities
- Efficient photocatalyst for formulation of self-cleaning construction materials, such as concrete or mineral plasters
- Suitable for the construction of efficient dye-sensitized solar cells
- Efficient heat stabilizer for silicone vulcanizates at process temperatures to more than 200°C
- Improvement of the flammability protection of silicone vulcanizates
- Additive and raw material for ceramic and metal materials as bonding agent, sintering additive or structural component

2.4.2 Titanate nanotube [21-23]

Titanate nanotube (TiO_2 nanotube, TNT) is one of the promising nanostructured oxides with tubular structure. TiO_2 is well known as a wide gap semiconductor oxide. Therefore, the most promising characteristic of TiO_2 lies in its photochemical properties such as high photocatalytic activity.

So far, three main routes have been developed to make TNT, i.e., via templating, anodic oxidation and hydrothermal synthesis methods. Table 2.1 shows the advantages, disadvantages and internal diameter of nanotubes obtained from each method. The templating method allows to construct materials that have a regular and controlled morphology at the nano- and/or micro-scale via adjusting the morphology of the template. However, extensive applications of this method may be limited due to the cost, insufficient characterization of template and a concern over long-term

instability of TNT products. The anodizing approach can build highly ordered and crystallized array films of TiO_2 immobilized on a titanium foil surface with controllable pore size, good uniformity and conformability over large areas. However, this preparation process suffers from an environmental concern, as the anodization of Ti foil must be processed in highly toxic hydrofluoric acid aqueous solutions.

Hydrothermal synthesis is a common method widely used to prepare zeolite catalysts in industry. This method has been adapted to produce high yields of TNT with vast pore and nanotubular structure.

Table 2.1 Comparison of typical synthesis of TNT [21]

Synthesis method	Advantages	Disadvantages	Internal diameter (nm)/ length (μm)
Template method	1. Controlled scale of nanotubes via different templates 2. More desirable for practical application	1. An increase in the cost of materials and long-term instability 2. Complicated fabrication process tube morphology may be destroyed during fabrication process	2.5–6000/ 0.05–200
Anodic oxidation	1. More desirable for practical applications 2. Ordered alignment with high length-to-diameter ratio 3. Feasible for extensive applications	1. Mass production is limited 2. The utilization of highly toxic solvent such as HF 3. Highly expense of fabrication apparatus and difficult separation of TiO_2 array film from substrates	20–110/ 0.1–2.4

Table 2.1 (Continued) Comparison of typical synthesis of TNT

Synthesis method	Advantages	Disadvantages	Internal diameter (nm)/ length (μm)
Hydrothermal synthesis	1. Simple route to obtain nanotube morphology for large scale production 2. Several modifications can be used to enhance titanium nanotubes 3. High cation-exchange capacity and length-to-diameter ratio	1. Long reaction duration is needed 2. Highly concentrated NaOH must be added 3. Difficult in achieving uniform size 4. Thermal unstable	3–10/ 50–500

2.4.3 Titanate nanosheet [24-25]

Lepidocrocite-type structure refers to the structure of γ-FeOOH. The structure of the lepidocrocite titanate is $H_xTi_{2-x/4}Y_{x/4}O_4$ (x ~ 0.8, Y is the vacancy). The structure can be constructed from the edge sharing of $(Ti,M)O_6$ octahedra, which extends into the sheets or layers along the a- and c- directions of the orthorhombic unit cell as shown in Figure 2.4. These sheets stack together along the b-direction like a pile of paper, resulting in 2-dimensional crystallites with the preferred orientation along the b-axis. The sheet as an elementary unit is roughly 1.3-nm thick, having only 3 layers of atoms.

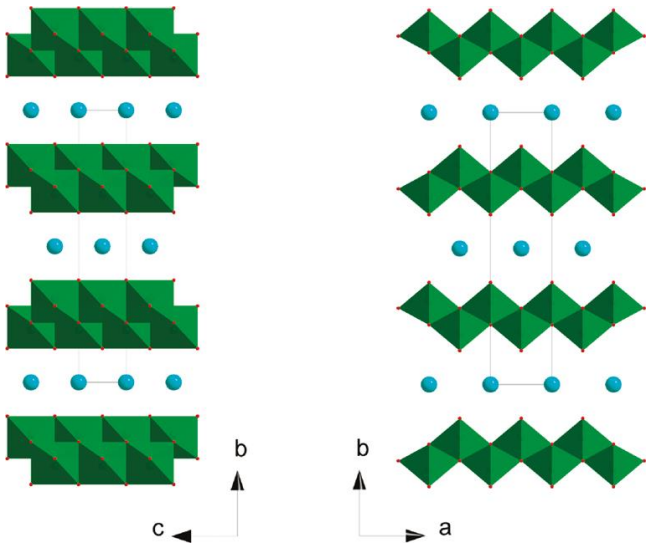

Figure 2.4 Polyhedral representation of the crystal structure for lepidocrocite titanates $A_xM_yTi_{2-y}O_4$. The green is represented the $(Ti,M)O_6$ units, whereas the blue dots are represented the alkali metal cations (M^{n+}) located between the layer [24]

The general composition of lepidocrocite titanates has the formula $A_xM_yTi_zO_4$, where A is usually an alkali metal, M is usually a transition metal having the valence not equal to +4, such as Zn or the cation vacancy. Because of the substitution of M^{n+} ($n < 4$) or the formation of the cation vacancy, the $(Ti,M)O_6$ layers become negatively charged. In order to preserve charge neutrality, alkali metal cations A^+ are usually incorporated between the layers. Lepidocrocite titanates can be easily synthesized by a conventional solid state synthesis from the mixture of metal carbonates/oxides.

Lepidocrocite titanates have excellent ion-exchange/intercalation reactivities. The A^+ cations originally located between the layers can be replaced by a wide variety of guest species, such as inorganic and/or organic cations, protons, and surfactants. The ion exchange of guest species into the layers with a consequence of the change in the distance between the layers is specifically called intercalation. In extreme cases, the intercalation of bulky molecules will pry apart the layers so that they become infinitely separated. The separation of stacks into individual layers is termed exfoliation. The reaction is facilitated by the increased interlayer separation in the H-form (In relative to the K-form), and also by the acid-base chemistry between the interlayer H^+ cations and the OH^- from the tetraalkylammonium hydroxide (TAAOH). The resulting

product is the colloidal aqueous suspension of the thin sheets, called titanium nanosheets (TNS).

2.5 Low density polyethylene [26-27]

Low density polyethylene (LDPE) is semi-crystalline polymer with excellent chemical resistance, good fatigue and wear resistance, and a wide range of properties due to differences in polymer chain length. LDPE provides good resistance to organic solvents, degreasing agents and electrolytic attack. It has a higher impact strength, but lower working temperatures and tensile strengths than polypropylene (PP). It is light in weight, resistant to staining and has low moisture absorption rate. This polymer offers good corrosion resistance and low moisture permeability. LDPE is also frequently used in consumer packaging, bags, bottles and liners.

Table 2.2 Typical properties of LDPE [27]

Property	ASTM	LDPE
Density (g/cm³)	D792	0.91-0.93
Tensile Strength (MPa)	D638	4.10-16.0
Tensile Modulus (GPa)	D638	0.10-0.26
Elongation at Yield (%)	D638	90-800
Hardness, Shore D	D785	55-59
Impact Strength (J/m)	D256	No break
Heat Deflection Temp (°C)	D648	38.0-49.0
Melting Temperature (°C)	D3418	98.0-120.0

2.6 Literature reviews

Theerakarunwong [28] studied the photodegradation with TiO_2. The photocatalytic efficiency of anatase and rutile of TiO_2 showed high effectively to remove organic matter. TiO_2 in anatase is more effective than that in rutile. Because rutile crystals lose their active surface area due to the higher synthetic temperature. The organic degradation mechanism depends on the adsorption rate on the surface of the catalyst. The charge variation is monitored by using the Zeta potential method. It was found that if TiO_2 has a high surface area, the rate of adsorption of organic

compounds increases. This results in higher organic degradation rates. The decomposition of methyl orange under UV light showed that 90% of methyl orange solution degraded within 1 hour.

Zhao et.al [12] prepared PE-TiO_2 composite films and their photocatalytic degradation under ultraviolet light and solar light in the ambient air was investigated. PE-TiO_2 composite film samples were casted with 0.02, 0.1 and 1.0 wt% TiO_2. PE-TiO_2 composite and pure PE samples were exposed under solar light at the ambient conditions for 20 and 100 hours. The pure PE samples and PE-TiO_2 composite samples before and after being irradiated at different times were all characterized by means of FT-IR and SEM techniques. The photocatalytic degradation process of PE-TiO_2 composite films was much faster than that of pure PE films under UV and solar light irradiations. The main products of PE-TiO_2 composite films via photocatalytic degradation process were CO_2 and H_2O. Their degradation rate was controlled by changing the loading of TiO_2 nanoparticles in the composite films.

Chen et.al [29] studied the degradation of methyl orange (C.I. Acid Orange 52), as a representative of an azo dye, by TiO_2. The results were compared with those obtained using TiO_2 nanocrystals prepared using a sol-gel method and a commercial sample, P25. BET surface area was characterized. The TiO_2-based nanocrystals prepared by the stearic acid gel method had BET surface area and photocatalytic activity greater than P25. The results indicated that the surface area and the proportion of photoactive components played an important role in the photodegradation reaction.

P.K. Roy et.al [30] studied an effect of photooxidation to degradation of LDPE with cobolt stearate at loading of 0.5, 1, 2, 3 and 5%wt. LDPE with cobolt stearate composite film sample were prepared by twin screw extruder then the films were fabricated by an extrusion blown film process. Composite samples were all characterized by tensile strength, %elongation at break, carbonyl index, morphology, molecular weight and %crystallinity. The results indicated that when cobolt stearate loading in LDPE was increased, carbonyl index and crack on film surface was also increase. Tensile strength, %elongation at break and molecular weight were decreased. However, %crystallinity was not change.

Kiatkittipong et.al [31] demonstrated that calcination of titanate nanostructures incited its transformation to various TiO_2 crystal phases and could improve

photoactivity. This study compared titanate nanotube phase transformation during calcination and their subsequent photodegradation. Titanate nanotube was synthesized via a hydrothermal method using P25. Structural characteristics of the products were investigated by transmission electron microscopy (TEM) and BET surface area analysis. As the calcination temperature was increased in the range of 200°C to 400°C the nanotubes became fragmented. Calcining at 500°C resulted in complete structural collapse of the nanotubes with the particles becoming a mixture of elongated and irregularly shaped morphologies. The optimum photoactivity occurred for samples calcined at 500°C with this temperature reflecting the transition between crystal phase and surface area.

Shibata et.al [32] studied photochemical properties of multi-layer films of titanium nanosheets. The band gap energy of nanosheets was reported to be 3.2 eV. The photocatalytic decomposition of gaseous 2-propanol and bleaching of methylene blue dye under UV light were measured. It was found that the photocatalytic decomposition activity of 2-propanol and methylene blue dye was quite low. In addition, the films exhibited a high photoinduced hydrophilic property.

Charasssrisoonthorn et.al [34] studied on degradation ability of LDPE films prepared with TiO_2 and TiO_2 coated with stearic acid (as dispersing agent). TiO_2 was calcined at 300°C, 350°C, 400°C and 450°C. Films were prepared by mixing LDPE with TiO_2 (1 phr) using an internal mixer then shaped with a compression molding machine. Films were put in UVA box for 200 hours. The results indicated that TiO_2 calcined at 300°C shown great photodegradation. TiO_2 exhibited low dispersion in LDPE due to non-polar of LDPE. A good dispersion of TiO_2 coated with steric acid in LDPE film was observed, hence, higher photodegradation.

Rattanapaiboonkit [35] reported the degradation of LDPE/TiO_2 composite films. TiO_2 was calcined at 300°C, 400°C and 500°C. Composite compounds were prepared by mixing LDPE with TiO_2 (1-3 php) using a twin-screw extruder then the films were fabricated by an extrusion blown film process. The photocatalytic degradation of films was performed in QUV (UVB radiation) for 12 days. It was found that intensity of anatase as compared to rutile phase for TiO_2 calcined at 400°C (T400) was higher than that of TiO_2 calcined at other temperatures. LDPE films with TiO_2 had poor TiO_2 dispersion due to difference in polarity between TiO_2 and LDPE. LDPE incorporated with T400 gave

the highest photodegradation as compared to LDPE films with TiO_2 calcined at other temperatures.

According to previous studies, catalyst band gap energy and surface area affects degradation ability. Catalyst that has low band gap energy and high surface area led to better degradation. Titanate nanotube and nanosheet have an interesting result in photoactivity and high surface area. Consequently, in this research studied effect of titanate nanostructures on photo degradation of LDPE film under UVA exposures. P25, titanate nanotube and nanosheet were characterized by TEM, XRD, BET DR-UV-vis. The photodegradable films with P25, titanate nanotube and nanosheet were shaped with a compression molding machine. Photodegradation was performed using UVA box. Photodegradable films properties were determined by TEM, DSC, carbonyl index (C.I.), %weight loss, color change (ΔE), %opacity and mechanical properties.

Chapter 3
Research methodology

3.1 Chemicals and materials

1. Low density polyethylene (LDPE): film grade LD2426K: (MFI 4.0 g/10 min (190°C, 2.16 kg)) InnoPlus by PTT Polyethylene Co., Ltd.
2. Titanium dioxide (TiO_2) Degussa P25: Fluka Sigma-aldrich Co., Ltd.
3. Potassium carbonate (K_2CO_3) Analytical grade: Carlo Erba reagent Co., Ltd.
4. Zinc oxide (ZnO) Analytical grade: Nano Materials Technology Co., Ltd.
5. Tetrabutylammonium hydroxide ($(C_4H_9)_4NOH$, TBAOH): Fluka Sigma-aldrich Co., Ltd.
6. Sodium hydroxide (NaOH) Analytical grade: Carlo Erba reagent Co., Ltd.
7. Hydrochloric acid (HCl) Analytical grade: Carlo Erba reagent Co., Ltd.
8. Methyl orange (MO): Labchem (Pty) Ltd.
9. Liquid N_2

3.2 Apparatus

1. Internal Mixer (PL2000/PL2001): C. Melcher & Co. (Thailand) Ltd.
2. Plastic grinder (Bosco A600): Bosco Engineering Co., Ltd.
3. Compression molding machine (MPGL 20 AT): Machgroup (1992) Co., Ltd.
4. Universal testing machine (LR 5K): LLOYD Instrument Co., Ltd.
5. Fourier transform infrared spectroscope (Spectrum Gx): Perkin Elmer Co., Ltd.
6. Differential scanning calorimeter (DSC7): Perkin Elmer Co., Ltd.
7. Thermogravimetric analyzer (TG209F3): Perkin Elmer Co., Ltd.
8. X-ray diffractometer (DMAX 2200/Ultima+): Rigaku Co., Ltd.
9. UV-visible spectrophotometer (T60): Bangkok High LAB Co., Ltd.
10. Diffuse reflectance UV-visible spectrometer (Helios alpha): Thermo electron Co., Ltd.
11. Colorimetric spectrophotometer (Miniscan XE plus): Hunter Lab Co., Ltd.
12. Brunauer–Emmett–Teller surface area analyzer (Autosorb-1): Quanta chrome Co., Ltd.
13. Field emission scanning electron microscope (JSM-7610F): JEOL Ltd.

14. Transmission electron microscope (JEM-2010): JEOL Ltd.
15. Stainless steel autoclave
16. Alumina crucible
17. Bunsen burner
18. Magnetic stirrer
19. Mechanical shaker (SSIC-25): SISCO India Co., Ltd.
20. Ultrasonic bath (LeelaSonic - 200): Leela Electronics Pvt. Ltd.
21. pH meter (827 pH Lab): Metrohm AG Co., Ltd.
22. Opacity meter (A822-2): Lenzing Instruments GmbH & Co. KG
23. Water aspirator with suction flask and buchner funnel
24. Analytical balance
25. Centrifuge
26. Freeze dryer machine (LGJ-10-3): Zhengzhou Nanbei Instrument Equipment Co. Ltd.
27. UVA Box with UVA lamps, PHILIPS TL-K 40W
28. Laboratory glassware/plastic
29. Tube furnace
30. Hot air oven

3.3 Preparation of catalysts

3.3.1 Preparation of titanate nanotube (TNT)

2 g P25 powder was added into 50 mL of 10 mol/L NaOH aqueous solution and the resulting mixture was stirred for 1 hour at room temperature. Then, the mixture was transferred to a stainless-steel autoclave and heated at 130°C for 24 hours. After cooled naturally in air, the white powder was thoroughly washed with HCl aqueous solution of 0.1 M and treated with distilled water, followed by drying in an hot air oven at 80°C [36].

3.3.2 Calcination of TNT

TNT was placed in the tube furnace to be calcined for 2 hours at 300, 400, 500 and 600°C which was labelled as TNT(300), TNT(400), TNT(500) and TNT(600), respectively.

3.3.3 Preparation of lepidocrocite titanate ($K_{0.8}Zn_{0.4}Ti_{1.6}O_4$)

K_2CO_3 was dried in an oven at 100°C overnight before use. The powder of K_2CO_3, ZnO and P25 that corresponding to the required stoichiometry for $K_{0.8}Zn_{0.4}Ti_{1.6}O_4$, were ground in a mortar for 20 minutes before being placed in an alumina crucible. The mixture was then heated in a furnace at 800°C for an hour, followed by the grinding. Then, the mixture was re-heated at 900°C for 20 hours and cooled naturally in air [37].

3.3.4 Proton exchange of $K_{0.8}Zn_{0.4}Ti_{1.6}O_4$

Potassium ions in $K_{0.8}Zn_{0.4}Ti_{1.6}O_4$ were replaced with protons by ion exchange. The $K_{0.8}Zn_{0.4}Ti_{1.6}O_4$ powder was magnetically stirred with 1 M HCl for 3 days (solid-to-solution ratio of 1 g to 100 mL). During the ion exchange, the acid was renewed everyday. Thereafter, the solid was filtered, washed with deionized water until free from excess acid, and then air dried at room temperature. A protonated form of the lepidocrocite titanate with the theoretical composition of $H_{1.6}Ti_{1.6}O_4 \bullet xH_2O$ was then obtained [24].

3.3.5 Exfoliation of $H_{1.6}Ti_{1.6}O_4 \bullet xH_2O$

0.40 g of the protonated form of the lepidocrocite titanate was reacted with the solution of TBAOH, setting the molar ratio of the TBA^+ cations in the solution to the proton in the solid to 1:1. The solid-to-solution ratio was at 0.4 g/100 mL. The mixture was mechanically shaken at 180 rpm for 14 days. The mixture initially comprising of solids and the clear colorless liquid was gradually transformed into a milky suspension within 14 days, indicating the exfoliation of lepidocrocite crystals into individual layers [24]. The suspension was freeze-dried and titanate nanosheet with tetrabutyl-ammonium ion (TNS/TBA^+) was then obtained.

3.4 Characterization of catalysts

3.4.1 Structural analysis

The crystalline phase of the catalyst was identified using x-ray diffractometer (XRD). 0.5 g of catalyst was packed on the sample holder (Cu Kα radiation, 40kV, 30 mA). The sample was scanned from 2θ of 5 to 80° with the rate of 0.02°/step and a scanning rate of 0.4 s/step. XRD pattern of sample was compared with XRD pattern of standard sample for the structure determination.

3.4.2 Surface area analysis

The surface area of the catalyst was identified using Brunauer–Emmett–Teller surface area analyzer (BET). 50 mg of catalyst was placed in sample cell. The sample cell was attached to the out gassing station at 300°C under vacuum condition for 12 hours. The sample cell was then removed from the out gassing station after the nitrogen filled and was attached to the analysis station. The equilibration time was set to 3 minutes and the adsorption was tested at the partial pressure (P/P_0) range of 10^{-6} to 1.0 at -195.6°C.

3.4.3 Proton exchange and exfoliation

Proton exchange of lepidocrocite titanate was determined by thermogravimetric analyzer (TGA). 10-20 mg of the protonated lepidocrocite titanate was loaded to the platinum pan. The sample was then heated from room temperature to 700°C at the heating rate of 10°C/min under the flow of nitrogen gas.

Exfoliation of $H_{1.6}Ti_{1.6}O_4 \cdot xH_2O$ was recorded by UV-visible spectrophotometer (UV-VIS). The solution after exfoliation was filled into a quartz cuvette. The wavelength was scanned from 200 to 900 nm.

3.4.4 Morphology

The morphology of catalysts was investigated by transmission electron microscopy (TEM). A small quantity of catalyst was dispersed in ethanol then sonicated for 30 minutes. Few drops of the resulting suspension were placed on a copper grid, followed by drying in a desiccator for 1 week. Then, catalysts were photographed with TEM at 100 kV.

3.4.5 Determination of band gap energy

The light absorption of catalyst was recorded by diffuse reflectance UV-visible spectrometer (DR-UV-vis). A small quantity of catalyst was placed on sample cell. The wavelength was used from 300 to 500 nm.

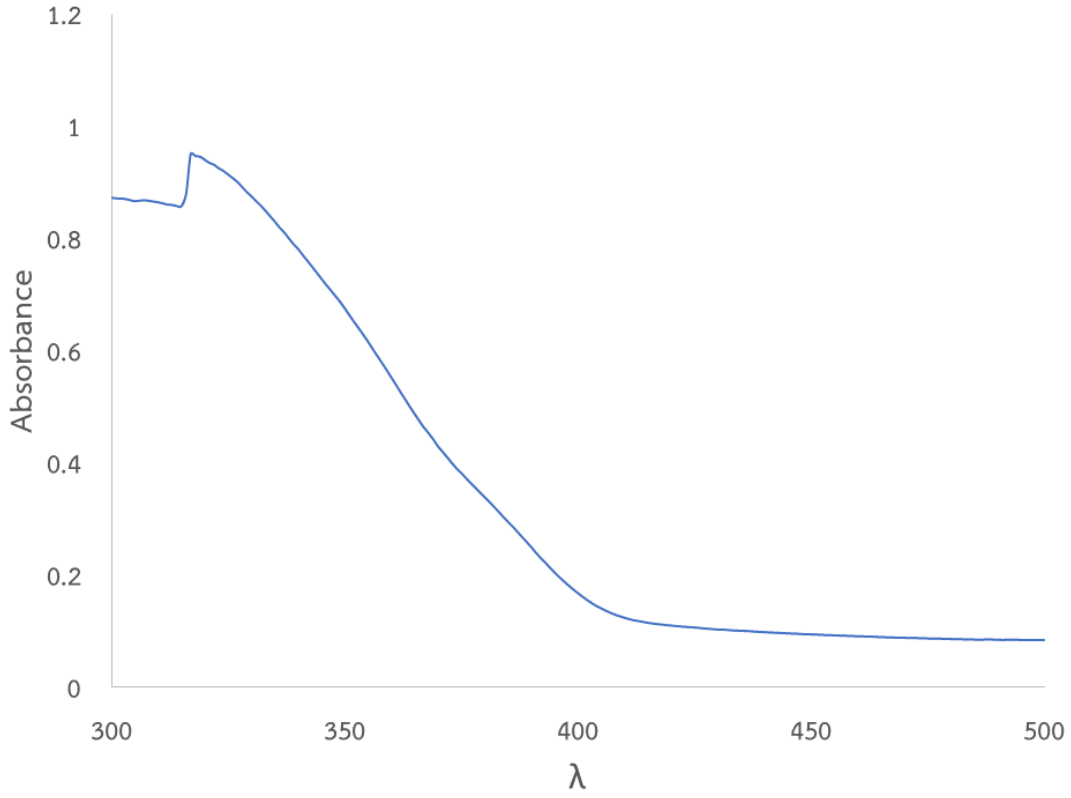

Figure 3.1 Diffuse reflectance UV-visible spectroscopy (DR-UV-vis) of P25

From DR-UV-vis graph (Figure 3.1), the slope of a graph was drawn and crossed x axis in order to defined λ. Thereafter, the band gap energy of catalyst can be calculated as shown in equation (3.1).

$$E_g = \frac{hc}{\lambda} \tag{3.1}$$

where E_g = Band gap energy (eV)

h = Planck constant (6.67×10^{-34} J.s)

c = Speed of light (3×10^{8} m/s)

λ = Light absorption wavelength (nm)

3.4.6 Photocatalytic oxidation of methyl orange (MO)

The photocatalytic activity of the catalyst was evaluated by photocatalytic oxidation of MO under UVA light irradiation using UVA lamps (PHILIPS TL-K 40W) as shown in Figure 3.2. 20 mg of the catalyst was mixed with 30 mL of 10 ppm MO solution that was further sonicated in the dark for 10 minutes in order to disperse

catalyst. Subsequently, it was magnetically stirred in the dark for 30 minutes to reach the adsorption equilibrium. During the photocatalytic reaction, samples were collected at 0, 10, 20 and 30 minutes and the catalyst was removed by centrifugation. The residual MO solution was tested by UV-VIS at 464 nm.

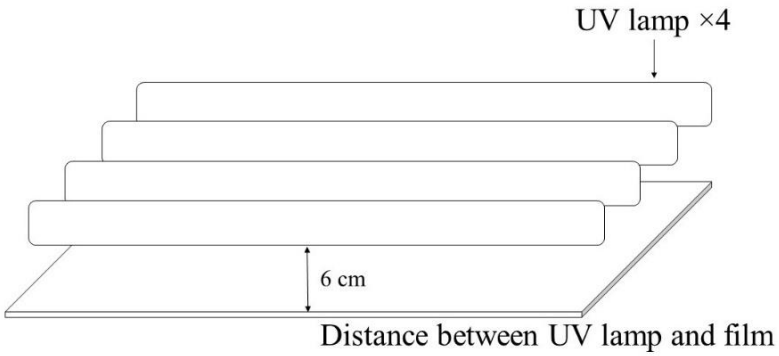

Figure 3.2 Configuration of UVA box

3.5 Films preparation

3.5.1 Preparation of compounds

Compounds were prepared by mixing 40 g of LDPE with P25, TNT(400) or TNS/TBA^+ at loadings of 0.5 and 1.0 phr using an internal mixer by condition as follows:

Temperature	170°C
Rotor speed	100 rpm
Mixing time	25 minutes

All compounds from an internal mixer were ground into small pieces by plastic grinder. All formulae are presented in Table 3.1

Table 3.1 Film formulae and compositions

Formula	LDPE (g)	P25 (g)	TNT(400) (g)	TNS/TBA^+ (g)
LD	40	-	-	-
LD/0.5P25	40	0.2	-	-
LD/1.0P25	40	0.4	-	-
LD/0.5TNT(400)	40	-	0.2	-
LD/1.0TNT(400)	40	-	0.4	-
LD/2.0TNS/TBA^+	40	-	-	0.8*

* From the calculation, loading of TNS is 0.5 phr.

3.5.2 Preparation of photodegradable films

The films were shaped with a compression molding machine by condition as follows:

Compound	1.5 g
Mold size	20×20×1 cm^3
Pressure	2000 psi
Temperature	220°C
Mold warmed up time	5 minutes
Compound warmed up time	8 minutes
Compression heating time	10 minutes
Compression cooling time	10 minutes
Cooling temperature	20°C

3.6 Characterization of photodegradable films

3.6.1 Catalyst loading in photodegradable film

A crucible was heated in a furnace at 600°C for 2 hours, followed by drying at room temperature before use. A compound was filled in a crucible about 2/3 of crucible height. Then, the crucible was burnt with a bunsen burner to eliminate organic component and subsequently, heated in a furnace at 600°C for 2 hours, followed by drying at room temperature and store in desiccator for 1 hour before weighing. A loading of catalyst can be calculated as shown in equation (3.2).

$$\text{Catalyst loading} = W_{after} - W_{before} \quad (3.2)$$

where W_{after} = Weight of crucible with compound before heat

W_{before} = Weight of crucible with residual

3.6.2 Thermal analysis of photodegradable film

The percentage of crystallinity of LDPE in photodegradable film was determined by differential scanning calorimeter (DSC) using condition as follows:

Film weight	10 mg
Temperature	25-150°C
Heating rate	20°C/min
Cooling rate	20°C/min
Gas	N_2

A calculation of %crystallinity is shown as equation (3.3).

$$\%\text{crystallinity} = \frac{\text{Normalized } \Delta H_f}{\Delta H_f^0} \times 100 \tag{3.3}$$

where ΔH_f = enthalpy of melting of polyethylene (J/g)

ΔH_f^0 = enthalpy of melting of 100% crystalline polyethylene (J/g) [26]

3.6.3 Morphology of photodegradable film

The morphology of the photodegradable films was investigated by field emission scanning electron microscopy (FESEM). A film was prepared by soaking in liquid N_2 for 20 min, followed by cracking under liquid N_2. Then, film was coated by gold. Cross section of coated films were photographed with FESEM at 10,000x.

3.6.4 Photodegradation of photodegradable film

The photodegradation of photodegradable film was performed using UVA box (Figure 3.2). The films with dimension of 6×8 cm^2 were placed in UVA box. During irradiation, films were collected sampling at 0, 50, 100, 150 and 200 hours.

3.6.5 Carbonyl index (C.I.)

Carbonyl index of photodegradable films before and after UVA exposures was measured by Fourier transform infrared spectroscopy (FT-IR) using attenuated total reflection method (ATR). The IR was analyzed from 650-4000 cm^{-1}. C.I. was calculated as equation (3.4).

$$\text{C.I.} = \frac{\text{Absorbance peak height at 1720 cm}^{-1}}{\text{Absorbance peak height at 729 cm}^{-1}} \tag{3.4}$$

3.6.6 %Weight loss

%Weight loss of photodegradable films before and after UVA exposures was evaluated using analytical balance. %Weight loss was calculated as equation (3.5).

$$\%\text{Weight loss} = \frac{W_0 - W_t}{W_0} \times 100 \tag{3.5}$$

where W_t = Weight after UVA exposure at sampling time (t)

W_0 = Weight before UVA exposure

3.6.7 Color change

Color change (ΔE) of photodegradable film before and after UVA exposures was determined by colorimetric spectrophotometer by D65/10°, L*, a* and b*. Colorimetric spectrophotometer was standardized using white and black tiles. Calculation of the color change was carried out as equation (3.6).

$$\Delta E = (\Delta L^{*2} + \Delta a^{*2} + \Delta b^{*2})^{1/2} \tag{3.6}$$

where ΔL* = L* after UVA exposure - L* before UVA exposure

Δa* = a* after UVA exposure - a* before UVA exposure

Δb* = b* after UVA exposure - b* before UVA exposure

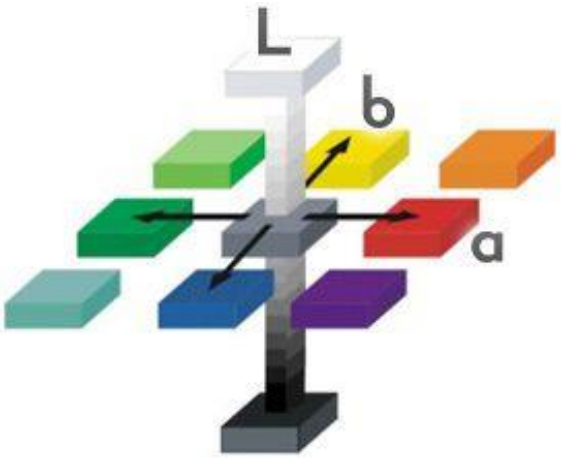

Figure 3.3 Three-dimensional model of L*, a* and b* color [38]

3.6.8 Film opacity

The opacity of photodegradable films before and after UVA exposures was measured by opacity meter.

3.6.9 Mechanical properties

Mechanical properties of photodegradable films before and after UVA exposures such as tensile strength at break, %elongation at break and Young's modulus were measured by Universal testing machine (UTM) according to ASTM D882 [39]. Films were tested using following conditions.

Specimen size	10×80 mm^2
Crosshead speed	100 mm/min
Gauge length	25 mm
Load cell	100 N
Number of sample	10

Chapter 4
Main Results and Discussion

This research studied the effect of TiO_2 nanostructures on photodegrability of LDPE films mixed with P25, titanate nanotube (TNT) and titanate nanosheet (TNS). The experiment was divided into 2 sessions: synthesis and characterization of catalysts and preparation and characterization of photodegradable films.

4.1 Synthesis and characterization of catalysts

4.1.1 Morphology of catalysts

TNT was synthesized from P25 by hydrothermal synthesis. Morphology of P25 and TNT were analyzed by TEM as shown in Figure 4.1. TNT was successfully prepared and clearly revealed an open-end structure that the outer and inner diameter of the final product was approximately in nm scale.

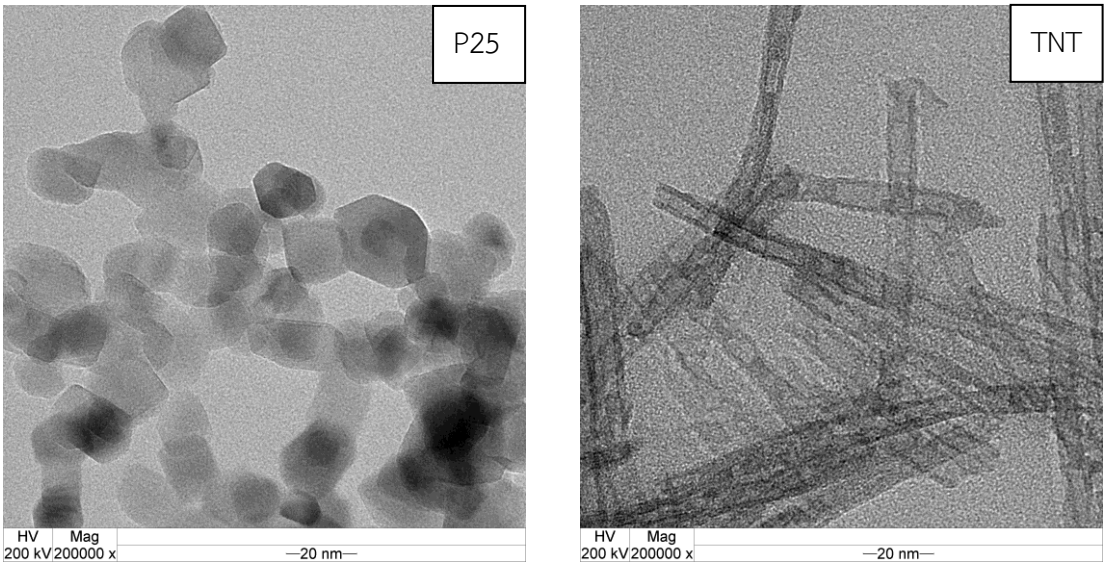

Figure 4.1 TEM images of P25 and TNT

4.1.2 Proton exchange and exfoliation

From the TGA of the initial lepidocrocite titanate (in the potassium form), it can be noted that it did not change in mass loss (Figure 4.2a). This is because the bulky sheets stack up together and linked by K^+, leading to no decomposition at 700°C. This resulted in not unexpected since the material was synthesized at a higher temperature

(i.e., 900°C). However, proton exchange of lepidocrocite titanate resulted in two regions of the mass loss (Figure 4.2b). The first loss was at 50-100°C due to evaporation of water molecules intercalated between the layers. The second loss was at 120-500°C owing to dihydroxylation and subsequent decomposition of the layered structure [24]. It is implied that proton exchange of lepidocrocite titanate was occurred. Therefore, lepidocrocite titanate was successfully prepared. K^+ in lepidocrocite titanate was replaced with H^+ (or hydronium ion) by proton exchange.

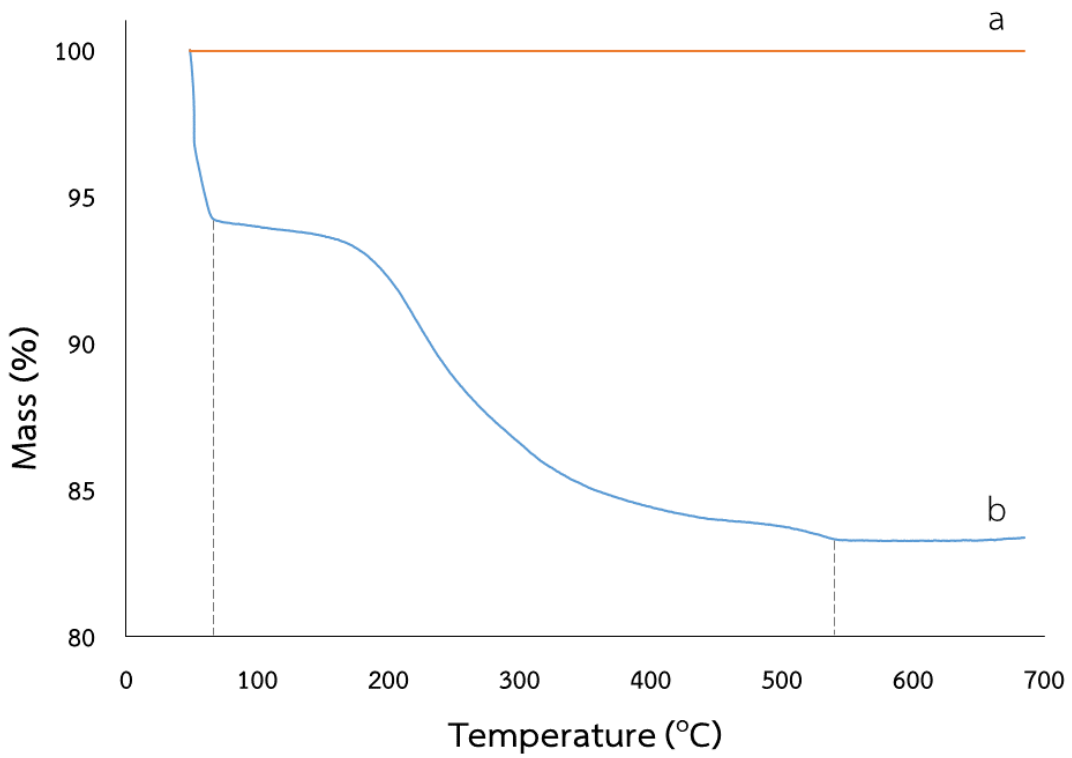

Figure 4.2 TGA curves of (a) Lepidocrocite titanate and (b) Protonated form of lepidocrocite titanate

Exfoliation of protonated form of lepidocrocite titanate into individual layers was accomplished by the mechanical shaking of protonated form with TBAOH (180 rpm) for 14 days. The starting mixture appeared as the sedimentation of white powder in water of left still (Figure 4.3a). The mixture revealed no UV-vis as expected for the mixture of large particles in any media. This indicated that exfoliation has not taken place (Figure 4.4a). Then, the mixture gradually changed into a white suspension upon prolong shaking (Figure 4.3b). Colloidal suspension indicated the separation of titanate

nanosheet into individual layers. The suspension showed λ_{max} at 265 nm (Figure 4.4b). This is because individual layer of nanosheet as colloidal suspension had high surface energy that absorbed UV light. Therefore, the exfoliation of the nanosheet into individual layers was achieved.

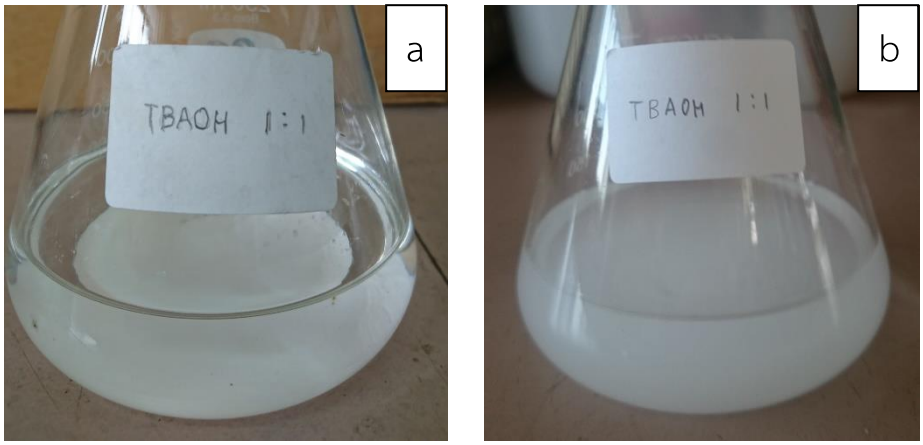

Figure 4.3 (a) Before and (b) After exfoliation of protonated form of lepidocrocite titanate

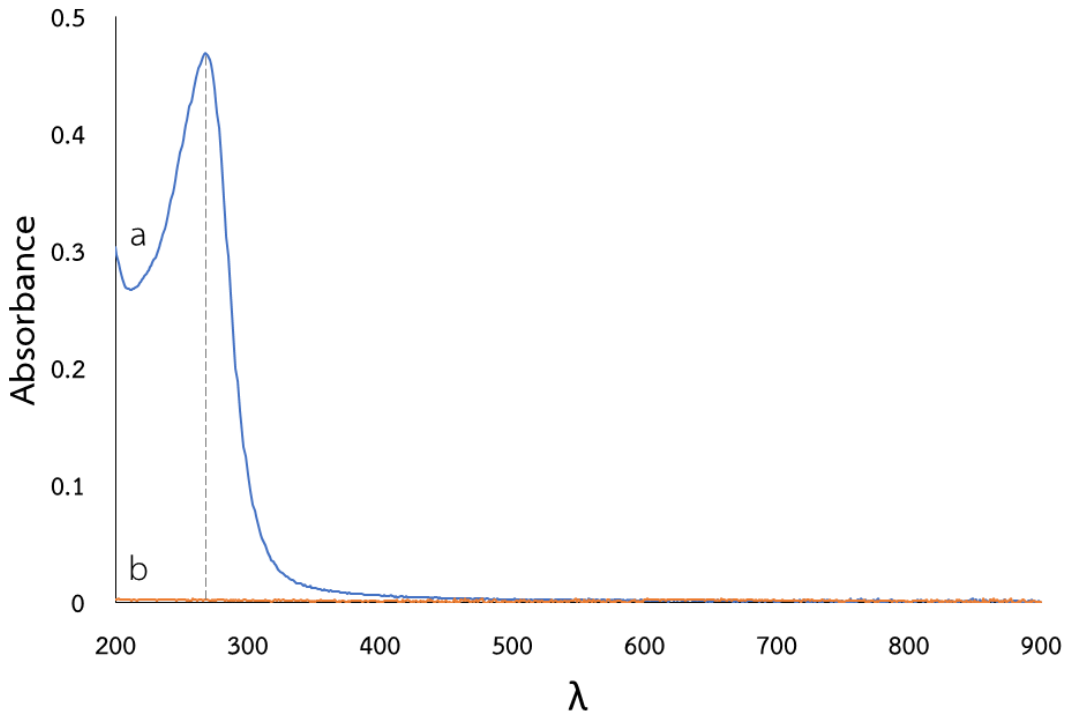

Figure 4.4 UV-visible spectroscopy (UV-vis) of TNS/TBA^+

4.1.3 Crystal Pattern of catalysts

Crystal patterns were analyzed by XRD as depicted in Figure 4.5. XRD patterns were described phase development of TNT during the process. Generally, P25 had mixed phases of anatase and rutile. Anatase phase had 2θ around 25° and 38° and rutile phase had 2θ around 27° and 36° (Figure 4.5a). TNT was synthesized from P25 by hydrothermal synthesis. Product was washed with HCl and led to Na^+ disappearance. In this step, nanosheet-like morphology can be obtained, which is considered as the TiO_2 nanosheet. Consequently, catalyst was treated with distilled water, then nanosheet was converted to be a tubular structure by scrolling process in order to reduce the surface energy [3]. TNT is consisted of amorphous and crystalline phases at 2θ around 24° and 48° (Figure 4.5b). Moreover, intensity of anatase phase was dramatically reduced. So disappearance of rutile phase was observed. Subsequently, calcined TNT for 2 hours at 400°C (Figure 4.5c) demonstrated amorphous phase was turn into crystalline phase. Thus, peak of anatase phase was sharply detected at 2θ around 25° and 38°.

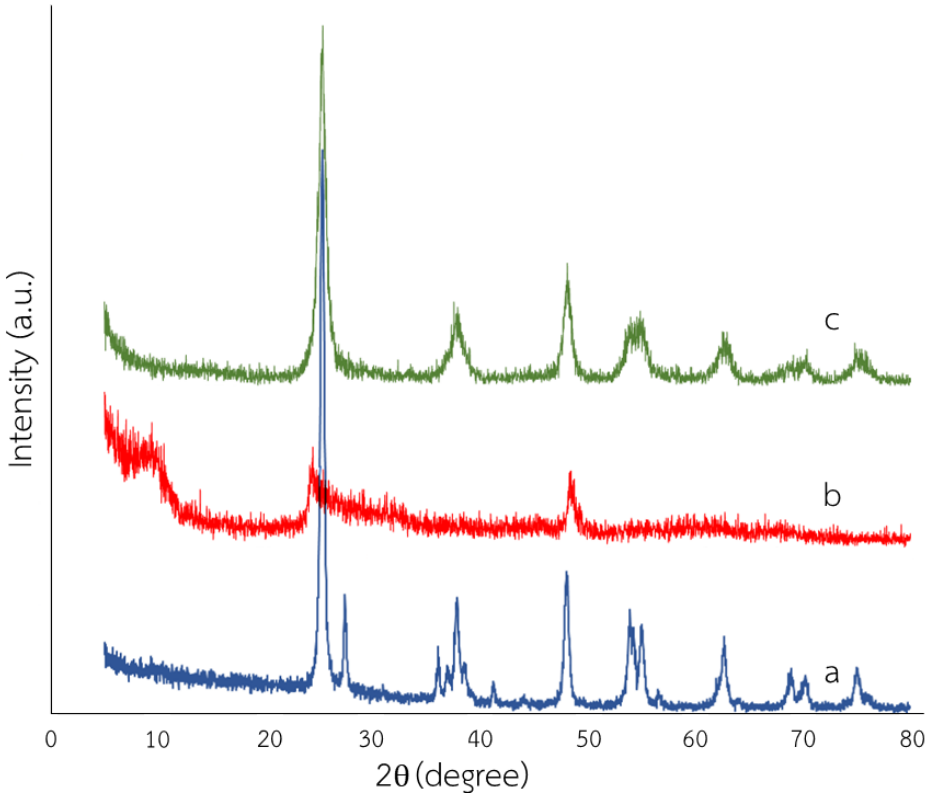

Figure 4.5 XRD patterns of (a) P25 (b) TNT and (c) TNT(400)

Crystal patterns of lepidocrocite titanate, proton exchange of lepidocrocite titanate and TNS/TBA^+ were analyzed by XRD as shown in Figure 4.6. Lepidocrocite titanate was synthesized by a solid state method. The sharp peaks in the XRD pattern as shown in Figure 4.6a indicated a high crystallinity of this material. After proton exchange (Figure 4.6b), peaks of 2θ around 12° indicating of the layered potassium titanate ($K_{0.8}Zn_{0.4}Ti_{1.6}O_4$) is shifted toward a lower 2θ. It is suggested that expansion of lepidocrocite titanate layer was obtianed. Thus, water molecules were intercalated into the interlayer space of the protonic titanate ($H_{1.6}Ti_{1.6}O_4 \bullet xH_2O$), which can be proved from TGA analysis (Figure 4.2b). XRD pattern of the exfoliated protonic titanate (by tetrabutylammonium hydroxide, TBAOH), after freeze drying, as presented in Figure 4.6c, shows an increase interlayer spacing. Hence, titanate nanosheet peak is shifted toward a lower 2θ in comparison to protonic titanate, likely due to the incorporation of TBA^+. This also indirectly suggested that the delamination of the layered crystals into individual layers was achieved, which was previously proved from UV-vis spectroscopy (Figure 4.4). Besides, bulky cations (TBA^+) created a larger gap between titanate layer, leading to the separation of nanosheets [25]. In addition, the peaks of the freeze-dried nanosheets are very broad, suggesting a limited number of restacked nanosheets. Proton exchange and exfoliation process of lepidocrocite titanate are illustrated in Figure 4.7.

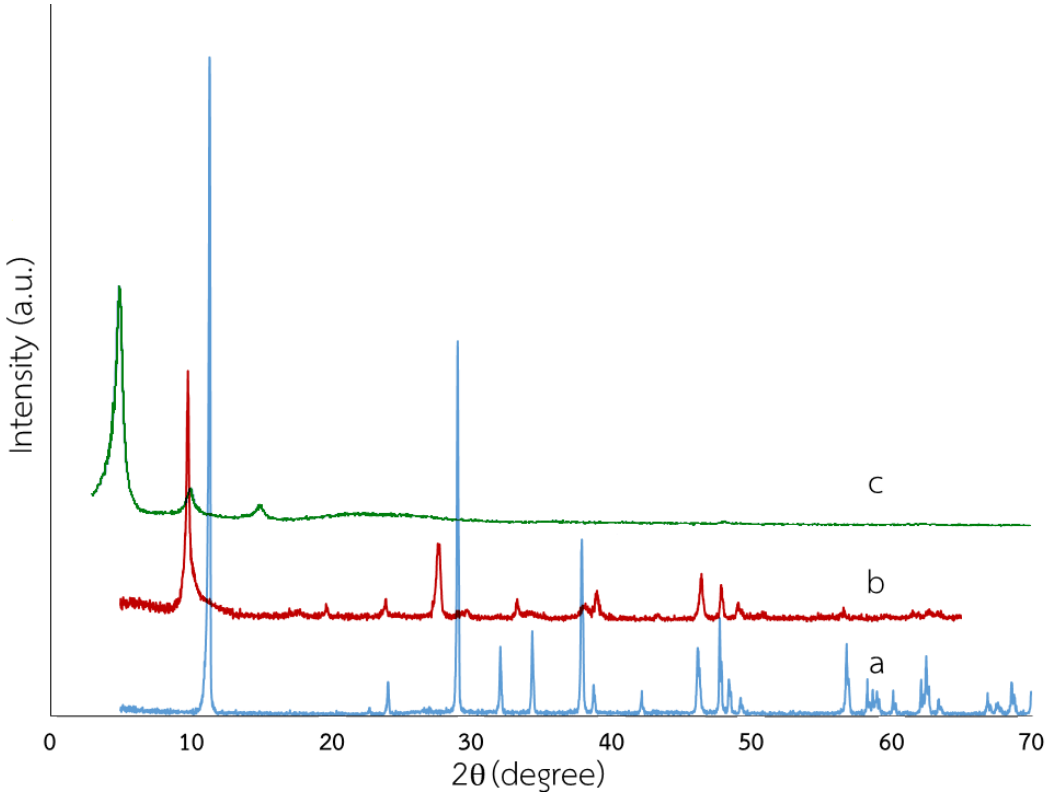

Figure 4.6 XRD patterns of (a) Lepidocrocite titanate (b) Protonated form of lepidocrocite titanate and (c) TNS/TBA^+

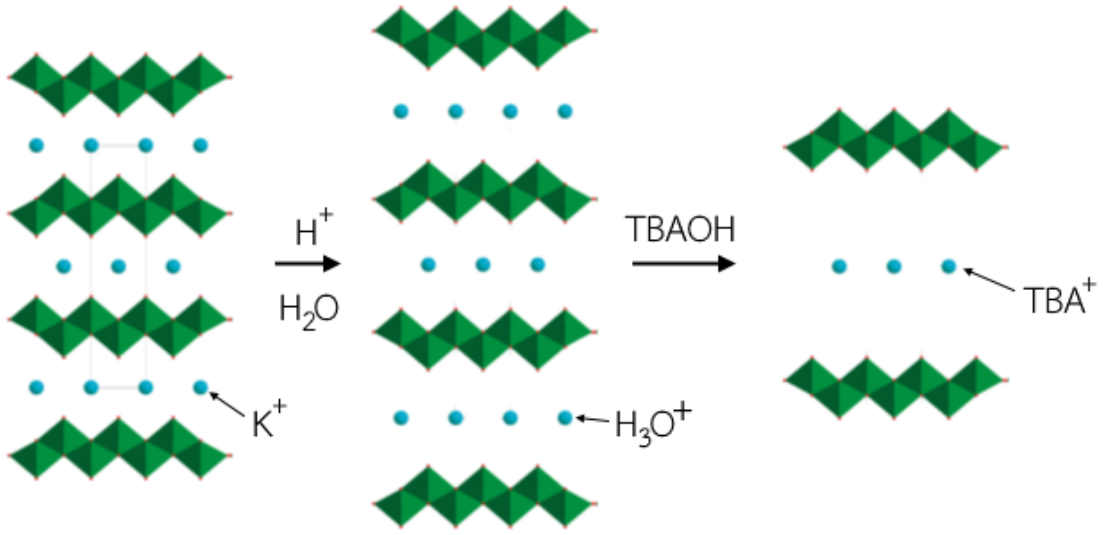

Figure 4.7 Proton exchange and exfoliation process of lepidocrocite titanate

4.1.4 Surface area analysis

The surface area of P25, TNT, TNT calcined for 2 hours at 400°C and TNS/TBA^+ were identified using BET surface area analyzer.

Table 4.1 Surface area of catalysts

Sample	Surface area (m^2/g)
P25	68.73
TNT	233.69
TNT(400)	201.48
Lepidocrocite titanate	3.41
TNS/TBA^+	192.94

From Table 4.1, it was found that surface area of TNT was higher than P25 due to structure change from spherical to tube-like with porous structure. After calcination, surface area of TNT(400) was decreased, as compared to TNT. It is assumed that, pore volume of TNT(400) was reduced [31].

Lepidocrocite titanate sheets were stacked together, resulting in a low surface area. After exfoliated by TBA^+, delamination of the layered into individual layers gave higher surface area than lepidocrocite titanate.

4.1.5 Determination of band gap energy

The light absorption of P25, TNT(400) and TNS/TBA^+ were recorded by DR-UV-vis. Thereafter, the band gap energy of catalyst can be calculated as described in session 3.4.5 (Figure 4.8). P25 had higher light absorption wavelength (**λ**), resulting in a lower band gap energy (E_g) that is summarized in Table 4.2.

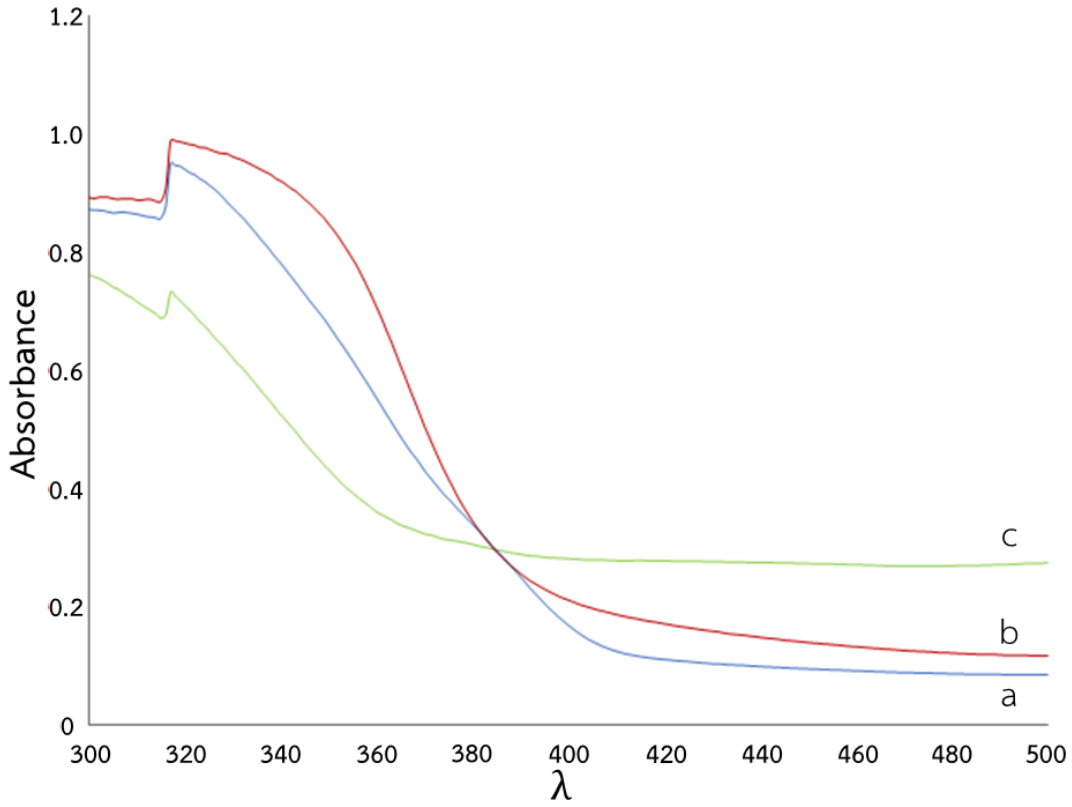

Figure 4.8 Diffuse reflectance UV-visible spectroscopy (DR-UV-vis) of (a) P25 (b) TNT(400) and (c) TNS/TBA^+

Table 4.2 Absorption wavelength and band gap energy of catalysts

Sample	Absorption wavelength (nm)	Band gap energy (eV)
P25	412	3.01
TNT(400)	397	3.12
TNS/TBA^+	395	3.14

Band gap energy of TNT(400) and TNS/TBA^+ were higher than P25 that revealed band gap energy of 3.01 eV owing to high intensity of anatase phase and mixed phases of rutile. An increase in band gap energy of TNT(400) to 3.12 eV indicated that structural and crystal of catalyst changed. Moreover, it can be noted that TNT(400) had lower anatase intensity with disappearance of rutile phase, as compared to P25 (Figure 4.5).

TNS/TBA^+ had large gap between titanate layer because it was separated into individual layer, which made the absorbance range and band gap energy of catalyst higher than that of P25.

4.1.6 Photocatalytic oxidation of methyl orange (MO)

The photodegradation activity of the catalyst in Figure 4.9 shows photocatalytic degradation of MO (C = concentration of MO at sampling time and C_0 = concentration of MO at initial time). Concentration of MO was reduced after UVA exposure. Calcination of TNT, it can be seen that the concentration of MO for TNT(400) decreased, as compared to those of TNT, TNT(300), TNT(500) and TNT(600) owing to an increase in anatase phase [3]. Hence, an increment of photocatalytic activity of TNT(400) was achieved. Therefore, TNT(400) was selected to investigate an effect of loading at 0.5 phr. The concentration of MO for TNS/TBA^+ was decreased slightly because of high band gap energy. The concentration of MO for P25 was lowest in comparison with other catalysts. The higher photocatalytic activity of P25 was attained because of its mixed phases (Anatase and rutile). Moreover, anatase and rutile phases induced the high photocatalytic activity because anatase phase could generate electron more than rutile phase due to low band gap energy. However, rutile phase can reduce the electron-hole pair recombination, which in turn facilitates the photocatalytic activity of the P25. [40]

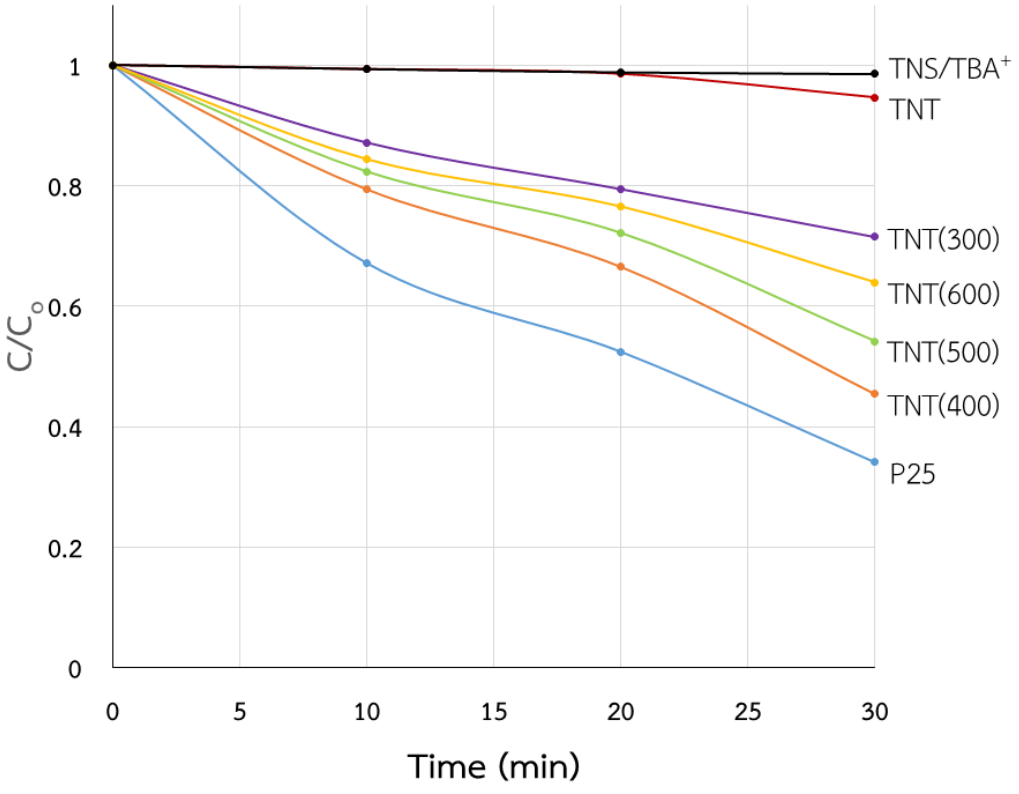

Figure 4.9 Photocatalytic oxidation of methyl orange (MO) under UVA irradiation

4.2 Preparation and characterization of photodegradable films

4.2.1 Effect of catalyst types

Compounds were prepared by mixing 40 g of LDPE with P25, TNT(400) at loading of 0.5 phr and TNS/TBA^+ at loading of 2.0 phr (TNS at loading of 0.5 phr).

Catalyst loading in photodegradable films was determined by burning with a bunsen burner. Catalyst loading in photodegradable films had similar catalyst loading as defined loading (Table 4.3).

Table 4.3 Catalyst loading in photodegradable films

Sample	Loading (phr)
LD/0.5P25	0.53
LD/0.5TNT(400)	0.52
LD/2.0TNS/TBA^+	0.57

4.2.1.1 Morphology of photodegradable film

Morphology of photodegradable films was evaluated by FESEM at 10,000x. The distribution of catalysts in LDPE films is depicted in Figure 4.10.

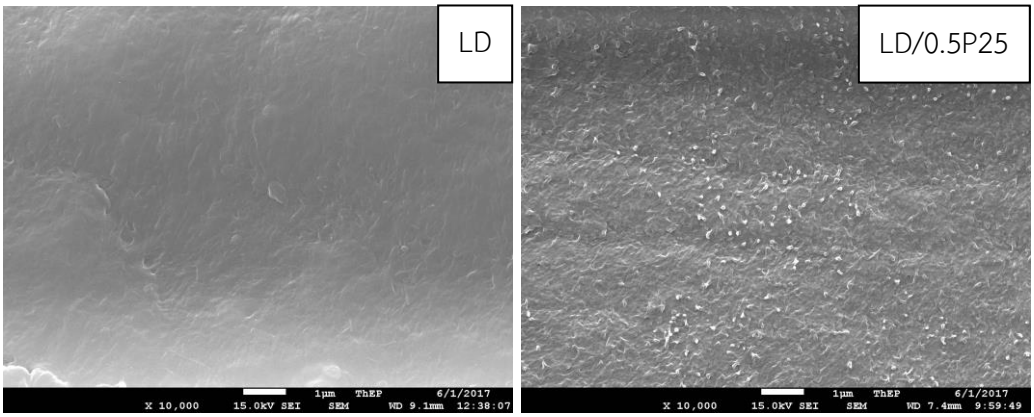

Figure 4.10 FESEM images of LD, LD/0.5P25, LD/0.5TNT(400) and LD/2.0TNS/TBA^+

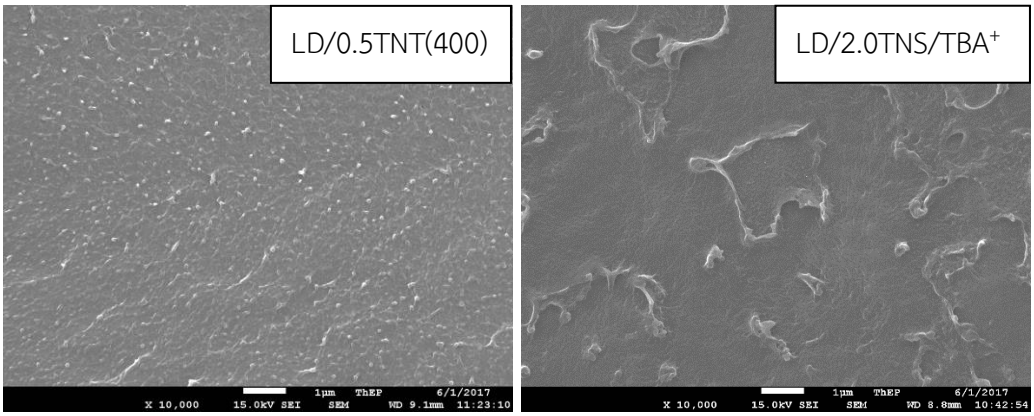

Figure 4.10 (Continued) FESEM images of LD, LD/0.5P25, LD/0.5TNT(400) and LD/2.0TNS/TBA^+

SEM images of LDPE mixed with P25 and TNT(400) had poor dispersion and distribution that could observe with white dots in LDPE films. This is because of differences in polarity between LDPE and P25 or TNT(400). On the other hand, TNS/TBA^+ could not exist in LDPE phase because TBA^+ and LDPE were non-polarity. Therefore, TNS/TBA^+ had good compatibility and dispersion with LDPE, resulting in no phase separation from this magnification.

4.2.1.2 Thermal analysis of photodegradable film

Thermal properties of photodegradable films were determined by DSC as illustrated in Table 4.4.

Table 4.4 Thermal properties of photodegradable films

Sample	T_m (°C)	ΔH_f (J/g)	% Crystallinity
LD	112	46.87	16
LD/0.5P25	113	48.41	16
LD/0.5TNT(400)	113	49.94	17
LD/2.0TNS/TBA^+	113	47.12	16

From the results of thermal properties, melting temperature (T_m) of photodegradable films with and without catalyst had similar value as 112°C and

%crystallinity range of 16-17%. It is suggested that addition of catalyst in LDPE did not interfere crystallinity of LDPE.

4.2.1.3 Physical properties of photodegradable films

Carbonyl index (C.I.), %weight loss, color change (ΔE) and %opacity of LDPE, LDPE mixed with P25, TNT(400) at loadings of 0.5 phr and TNS/TBA^+ at loadings of 2.0 phr before and after UVA exposures at 0, 50, 100, 150 and 200 hours were determined.

Carbonyl index (C.I.)

Carbonyl functional group of photodegradable films before and after UVA exposures was recorded by Fourier transform infrared spectroscopy (FT-IR) using attenuated total reflection method (ATR). The IR was scanned from 650-4000 cm^{-1}. From ATR-FTIR spectra of LDPE with and without catalyst before and after UVA exposure (Examples in Figures 4.11 and 4.12), Carbonyl index (C.I.) can be calculated by area under absorbance peak at 1720 cm^{-1} (Carbonyl stretching peak) divided by area under absorbance peak at 729 cm^{-1} (C-H Rocking peak).

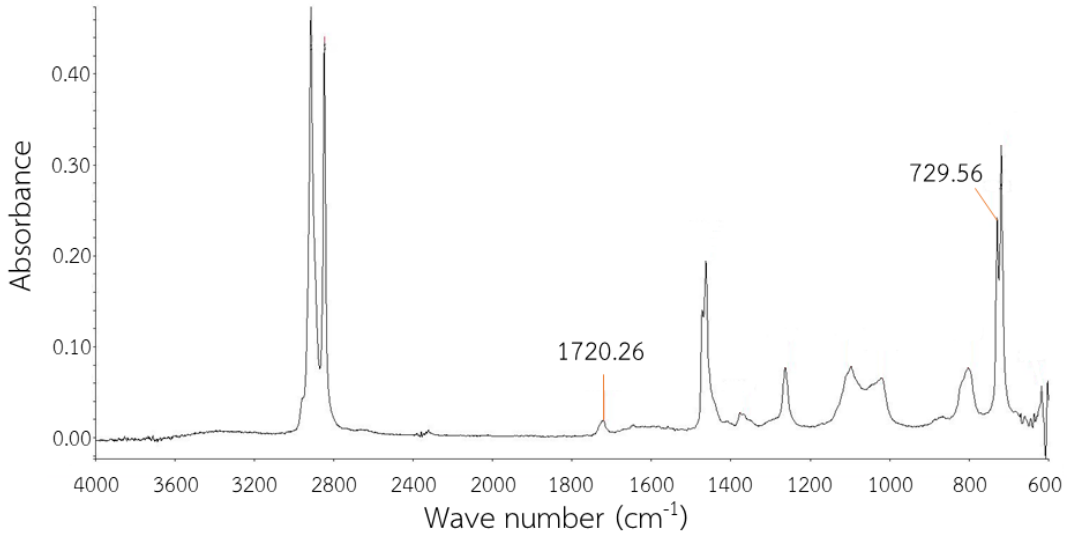

Figure 4.11 ATR-FTIR spectrum of LDPE film before UVA exposure

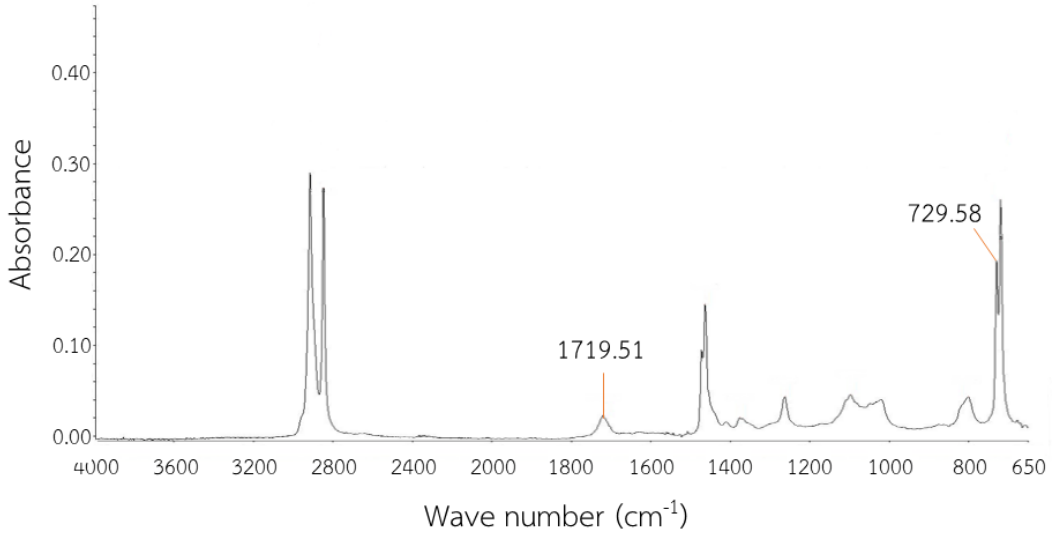

Figure 4.12 ATR-FTIR spectrum of LDPE film after UVA exposure

From the calculation, it is noticed that carbonyl index was increased after irradiation. This is because catalyst absorbed UV light and generated free electrons (e^-) and holes (h^+) in the conduction and valence bands, respectively. Subsequently, reaction with O_2 induced the formation of several active oxygen species such as •OH, O_2•-, and HO_2•. The active oxygen species as described above, initiated the degradation reaction by attacking neighboring LDPE chains and produced –(•CH_2CH_2)–. In addition, further interaction with O_2 promoted chain scission of LDPE chains and produced carbonyl groups [41].

Photodegradable films of LDPE with P25, TNT(400) at loading of 0.5 phr and TNS/TBA^+ at loading of 2.0 phr had the same catalyst loading at 0.5 phr. Carbonyl index of LDPE photodegradable films before and after UVA exposures are presented in Figure 4.13. The order of carbonyl index of LDPE mixed with P25 was higher than LDPE mixed with TNT, LDPE mixed with TNS/TBA^+ and LDPE film, respectively due to lower band gap energy of P25. Hence, numerous active species could generate, resulting in a better degradation.

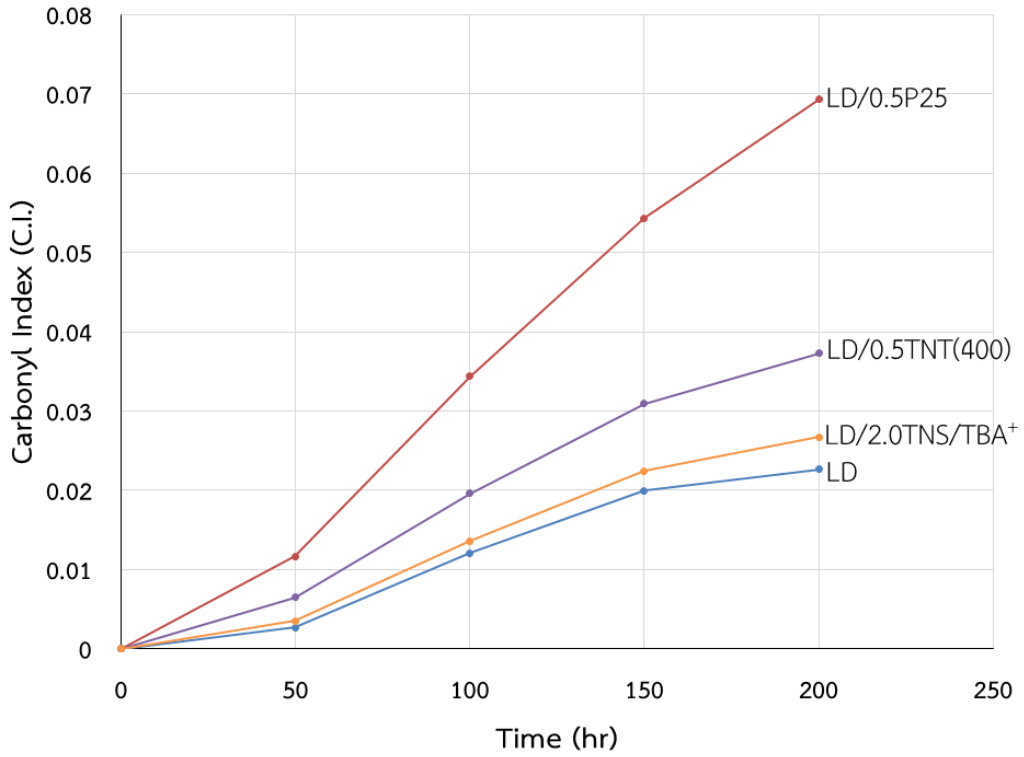

Figure 4.13 Carbonyl index (C.I.) of LD, LD/0.5P25, LD/0.5TNT(400) and LD/2.0TNS/TBA^+ at various UVA exposure times

%Weight loss

%Weight loss of photodegradable films before and after UVA exposures was evaluated using analytical balance as displayed in Figure 4.14. After UVA irradiation, photodegradable film had an increase in %weight loss. This is because catalyst absorbed UVA and generated electrons, leading to further interaction as described in session 4.2.1.3 (Carbonyl index). Therefore, chain scission of LDPE was occurred. Moreover, further degradation of carbonyl group could produce CO_2 and H_2O. Hence, volatile products of degradation had loss in the degradation process. %weight loss enhanced that agreed with the result of carbonyl index. So, the highest %weight loss of P25 was attained.

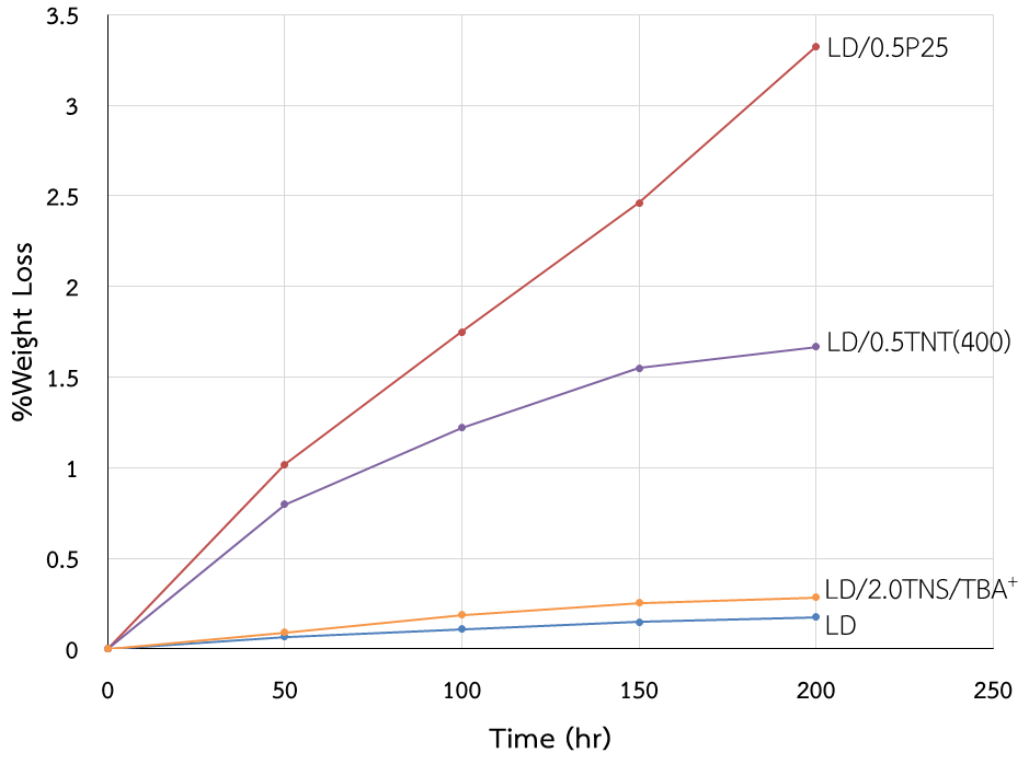

Figure 4.14 %Weight loss of LD, LD/0.5P25, LD/0.5TNT(400) and LD/2.0TNS/TBA^+ at various UVA exposure times

Color change (ΔE)

Additionally, color change (ΔE) and lightness change (ΔL) can be applied for investigation of photocatalytic degradation under UVA of all films. Color and lightness change of photodegradable films before and after UVA irradiation were evaluated by colorimetric spectrophotometer as illustrated in Figures 4.15-4.16. Color and lightness change were raised. Catalyst absorbed UVA and generated electrons, leading to further interaction as explained in session 4.2.1.3 (Carbonyl index). Carbonyl groups were formed by oxidation of LDPE by light absorption. Eventually, cracking of the film was existed that caused light scattering in the LDPE films, resulting in color and lightness change of photodegradable films. These results corresponded to an increment of carbonyl index and %weight loss.

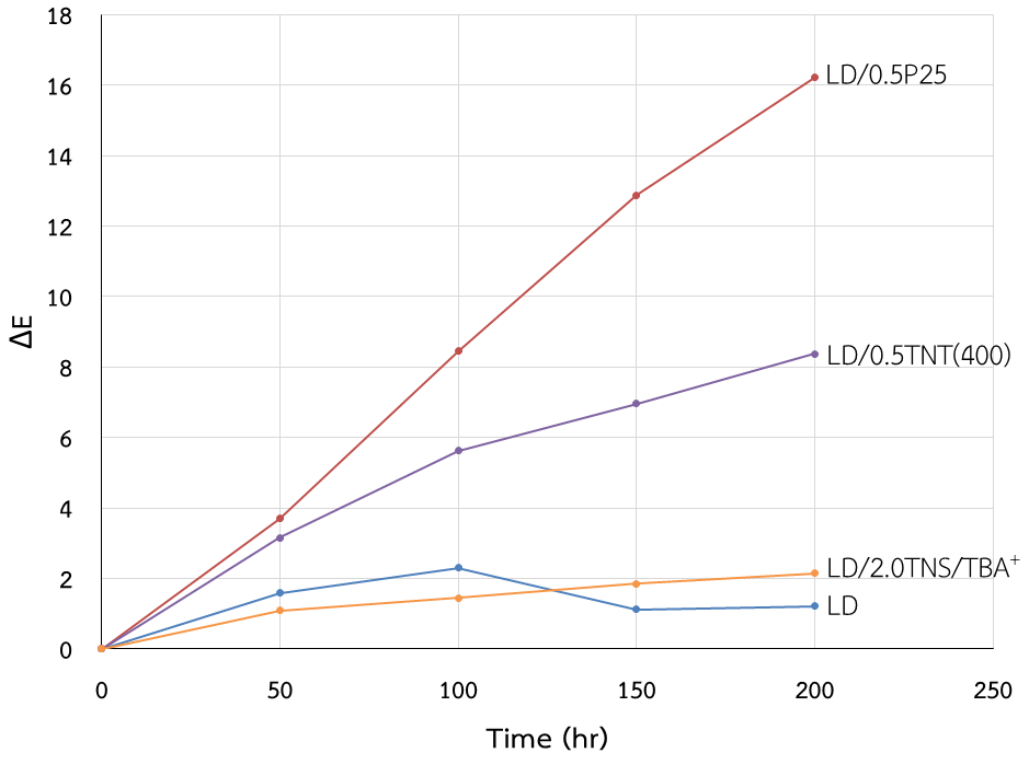

Figure 4.15 Color change (ΔE) of LD, LD/0.5P25, LD/0.5TNT(400) and LD/2.0TNS/TBA^+ at various UVA exposure times

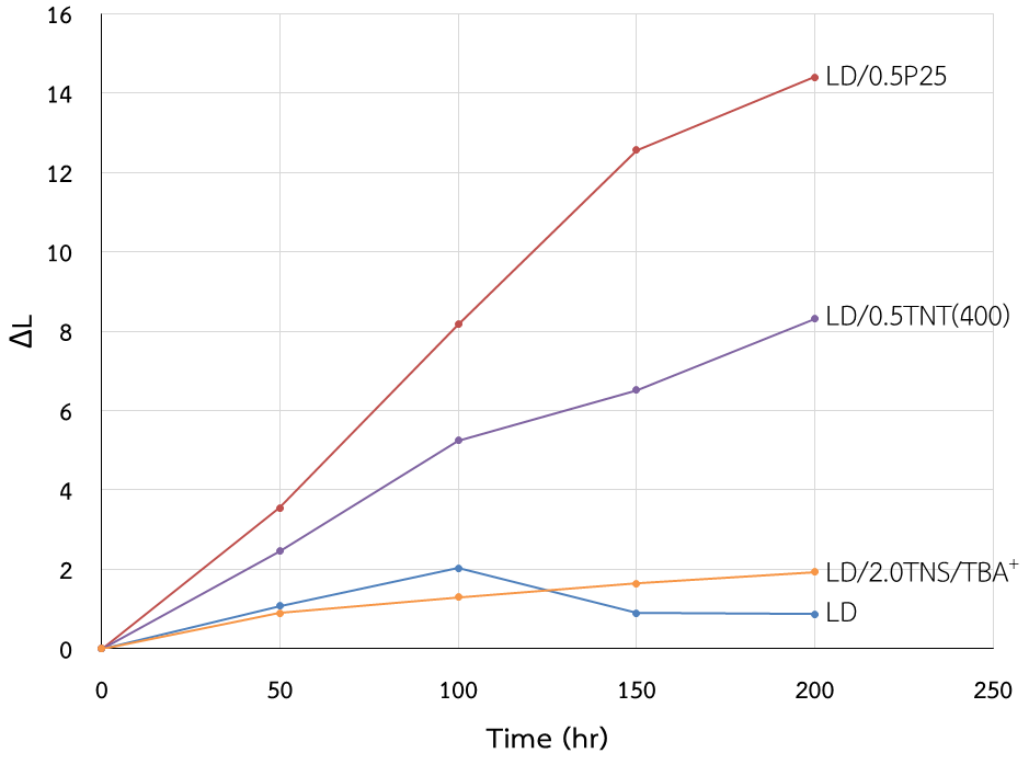

Figure 4.16 Lightness change (ΔL) of LD, LD/0.5P25, LD/0.5TNT(400) and LD/2.0TNS/TBA^+ at various UVA exposure times

Film opacity

Opacity of photodegradable films before and after UVA exposures was measured by opacity meter. The results are listed in Table 4.5.

Table 4.5 The opacity of LD, LD/0.5P25, LD/0.5TNT(400) and LD/2.0TNS/TBA^+ under UVA irradiation at 0 and 200 hours

Sample	Film opacity (%)		
	0 hr	200 hrs	%Difference
LD	24.3	25.8	6.2
LD/0.5P25	41.2	54.0	31.1
LD/0.5TNT(400)	31.8	40.1	26.1
LD/2.0TNS/TBA^+	30.7	33.4	8.8

The highest opacity value of LDPE mixed with P25 before UVA exposure was observed, as compared to LDPE film. This is because agglomeration of P25 (Figure 4.10) caused more light reflection and scattering in LDPE film. Therefore, low light transmission through LDPE film induced to high opacity. However, the opacity of an incorporated TNT(400) or TNS/TBA^+ in LDPE was lower than LDPE added P25. TNT structure had low refractive index of the films due to high porous of nanotube structure [42]. Thus, light reflection and scattering in LDPE film was reduced. TNS/TBA^+ exhibited good dispersion in LDPE as seen in Figure 4.10. Light is allowed to pass through and, hence, low light reflection and scattering in LDPE film was occurred. Opacity of photodegradable films with adding P25 or TNT(400) was increased after UVA exposure. In contrast, it can be indicated that the opacity of LDPE film added TNS/TBA^+ after UVA exposure did not vary significantly owing to good dispersion in LDPE but photocatalytic activity was declined. However, LDPE mixed with P25 or TNT(400) gave higher opacity than the films before UVA exposure. This is because catalyst absorbed UVA and generated electrons, leading to further interaction as explained in session 4.2.1.3 (Carbonyl index and color change). Cracking of the films from photodegradation effected higher light scattering in LDPE films, resulting in an increment of opacity of photodegradable films.

4.2.1.4 Mechanical properties of photodegradable films

Mechanical properties of photodegradable films before and after UVA exposures such as tensile strength at break, %elongation at break and Young's modulus were examined by Universal testing machine (UTM) as illustrated in Figures 4.17-4.19. LDPE film with and without catalyst before UVA exposures did not reveal a significant difference in tensile strength at break, %elongation at break and Young's modulus. This is because all the films had similar value in %crystallinity as represented in Table 4.4 and small amount of catalyst loading (0.5 phr) could not interfere in mechanical properties. LDPE films with and without catalyst after UVA exposures were not significant change in tensile strength at break and Young's modulus. However, %elongation at break was slightly increased. It can be implied that LDPE was organic materials but P25 and TNT were inorganic, leading to an incompatibility between LDPE and catalysts. Therefore, a decrease of transfer force between phases was occurred. On the other hand, TNS/TBA^+ had good dispersion in LDPE as depicted in Figure 4.10. Hence, mechanical properties of LDPE mixed with TNS/TBA^+ was similar to LDPE film. In addition, further interaction of active LDPE chain with O_2 induced chain scission phenomenon. On the other hand, active LDPE chain preferred to interact with each another to create crosslinked between LDPE chains. Therefore, LDPE films with and without catalyst had possibility of both chain scission and crosslink phenomena.

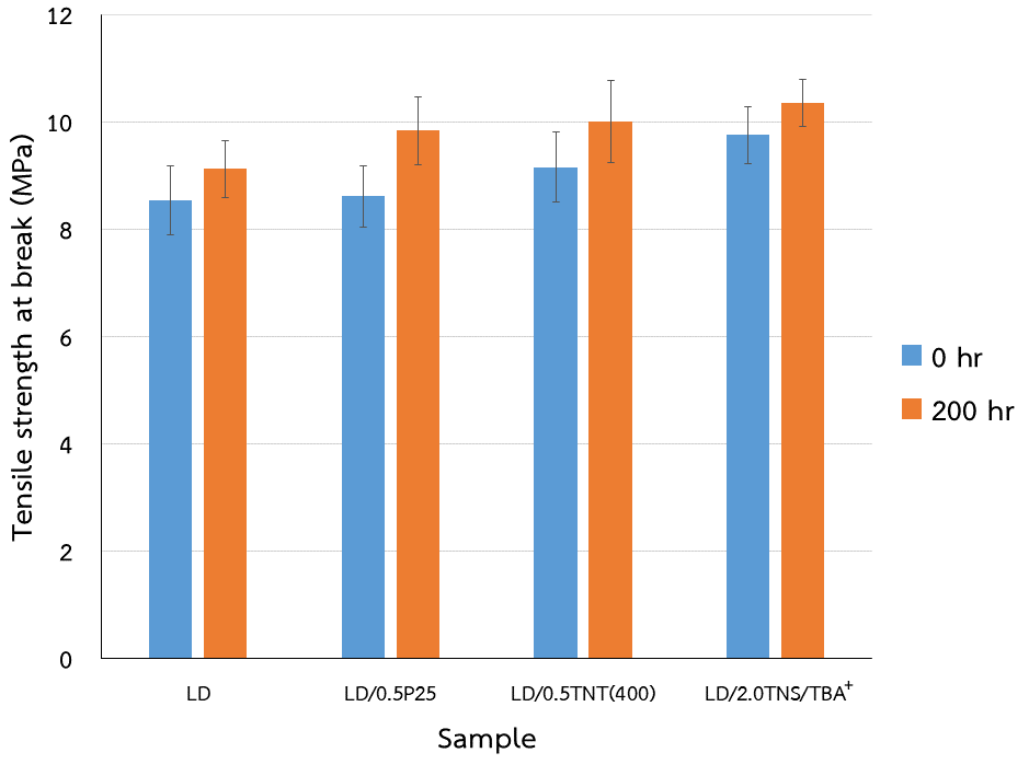

Figure 4.17 Tensile strength at break of LD, LD/0.5P25, LD/0.5TNT(400) and LD/2.0TNS/TBA^{+} under UVA irradiation at 0 and 200 hours

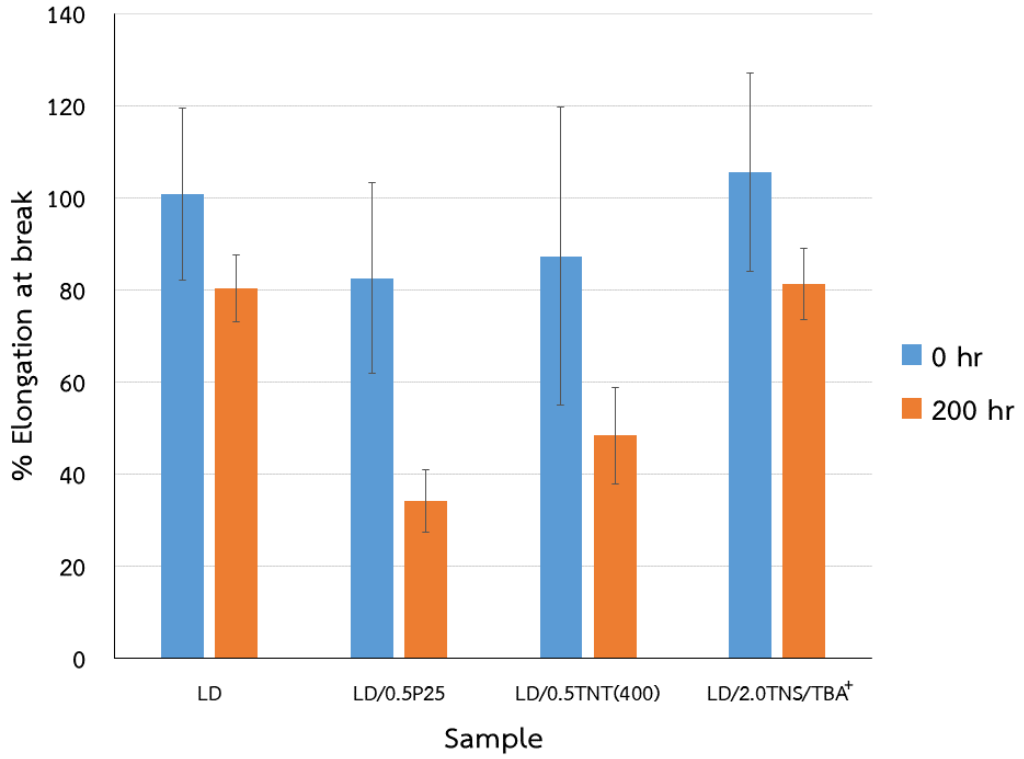

Figure 4.18 %Elongation at break of LD, LD/0.5P25, LD/0.5TNT(400) and LD/2.0TNS/TBA^{+} under UVA irradiation at 0 and 200 hours

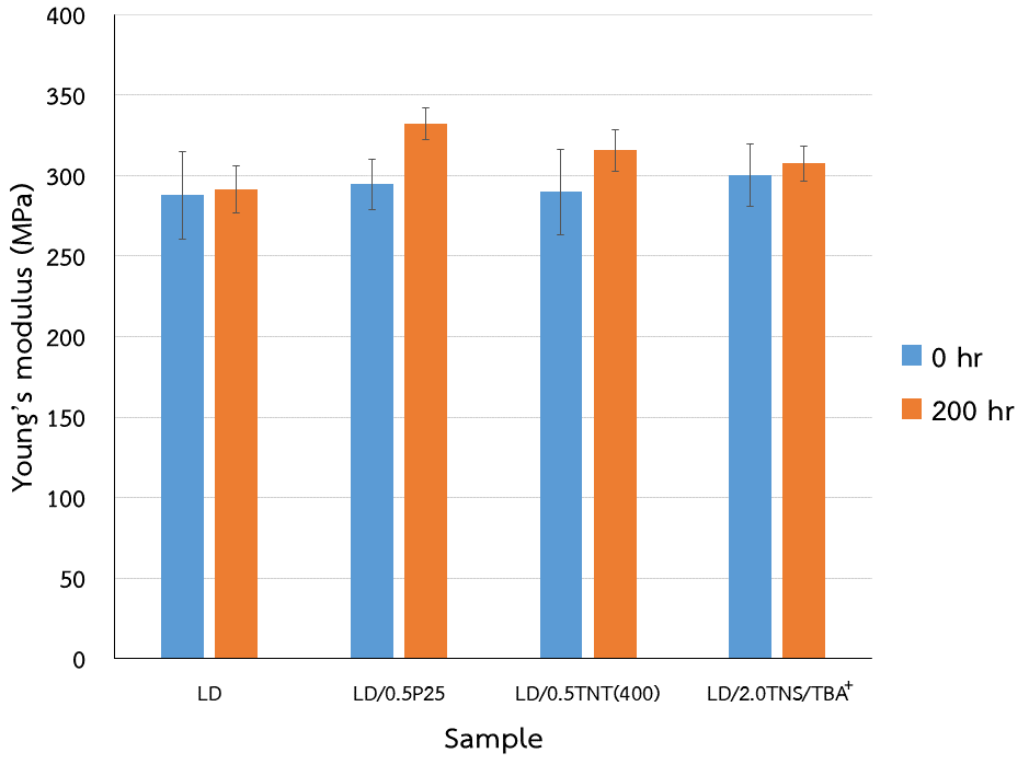

Figure 4.19 Young's modulus of LD, LD/0.5P25, LD/0.5TNT(400) and LD/2.0TNS/TBA^+ under UVA irradiation at 0 and 200 hours

According to LDPE film with TNS/TBA^+ had photocatalytic degradation result as similar to LDPE. Therefore, LDPE incorporated with P25 and TNT(400) were selected for investigation the effect of catalyst content.

4.2.2 Effect of catalyst content

P25 or TNT(400) was mixed with LDPE at loadings of 0.5 and 1.0 phr. Catalyst loading in photodegradable films was determined by burning with a bunsen burner. It was found that catalyst content in photodegradable films had similar amount as defined loading (Table 4.6).

Table 4.6 Catalyst loading in photodegradable films

Sample	Loading (phr)
LD/0.5P25	0.53
LD/1.0P25	1.06
LD/0.5TNT(400)	0.52
LD/1.0TNT(400)	1.08

4.2.2.1 Physical properties of photodegradable films

LDPE, LDPE mixed P25 and TNT(400) at loadings of 0.5 and 1.0 phr before and after UVA exposures at 0, 50, 100, 150 and 200 hours were examined. Carbonyl index of photodegradable films before and after UVA exposures was evaluated using FT-IR attenuated total reflection method (ATR) as depicted in Figure 4.20. %Weight loss of photodegradable films before and after UVA exposures are illustrated in Figure 4.21. Color change and lightness change of photodegradable film before and after UVA exposures are demonstrated in Figures 4.22-4.23. Photodegradation of the films were enhanced with catalyst loading from 0.5 to 1.0 phr. Therefore, carbonyl index, %weight loss, color and lightness change were escalated. It is implied that catalyst acted as an accelerator for degradation reaction. An increment amount of catalyst could absorb more UVA light, leading to larger amount of several active oxygen species such as •OH, O_2•- and HO_2• that enhanced the ability of film degradation.

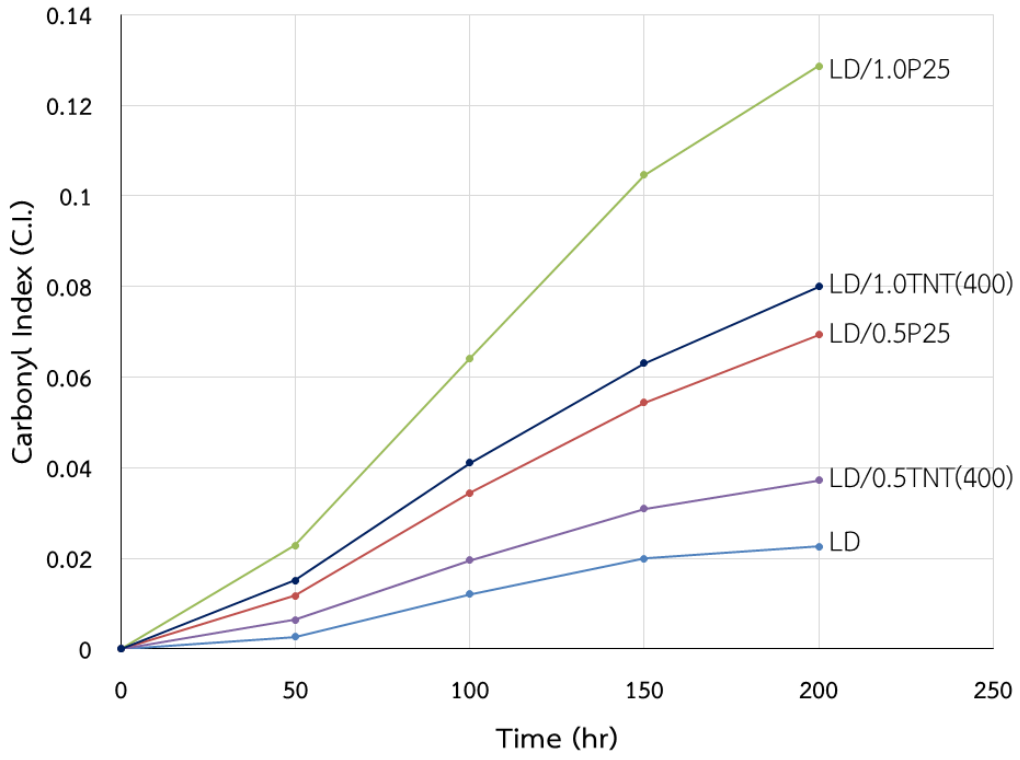

Figure 4.20 Carbonyl index (C.I.) of LD, LD/0.5P25, LD/1.0P25, LD/0.5TNT(400) and LD/1.0TNT(400) at various UVA exposure times

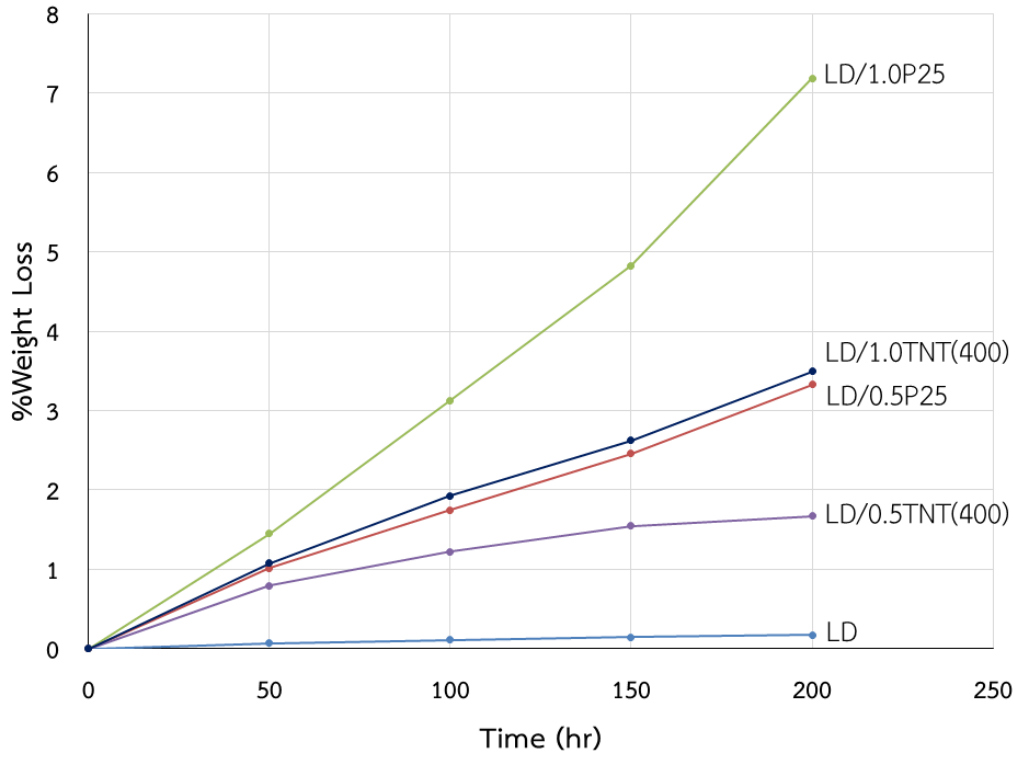

Figure 4.21 %Weight loss of LD, LD/0.5P25, LD/1.0P25, LD/0.5TNT(400) and LD/1.0TNT(400) at various UVA exposure times

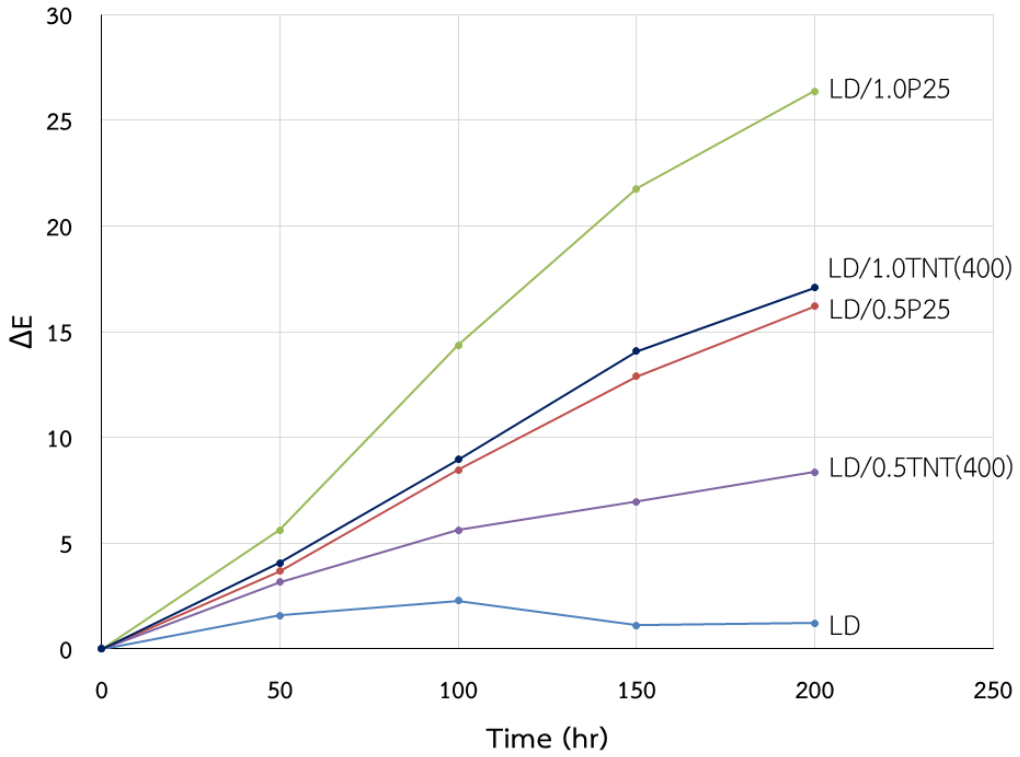

Figure 4.22 Color change (ΔE) of LD, LD/0.5P25, LD/1.0P25, LD/0.5TNT(400) and LD/1.0TNT(400) at various UVA exposure times

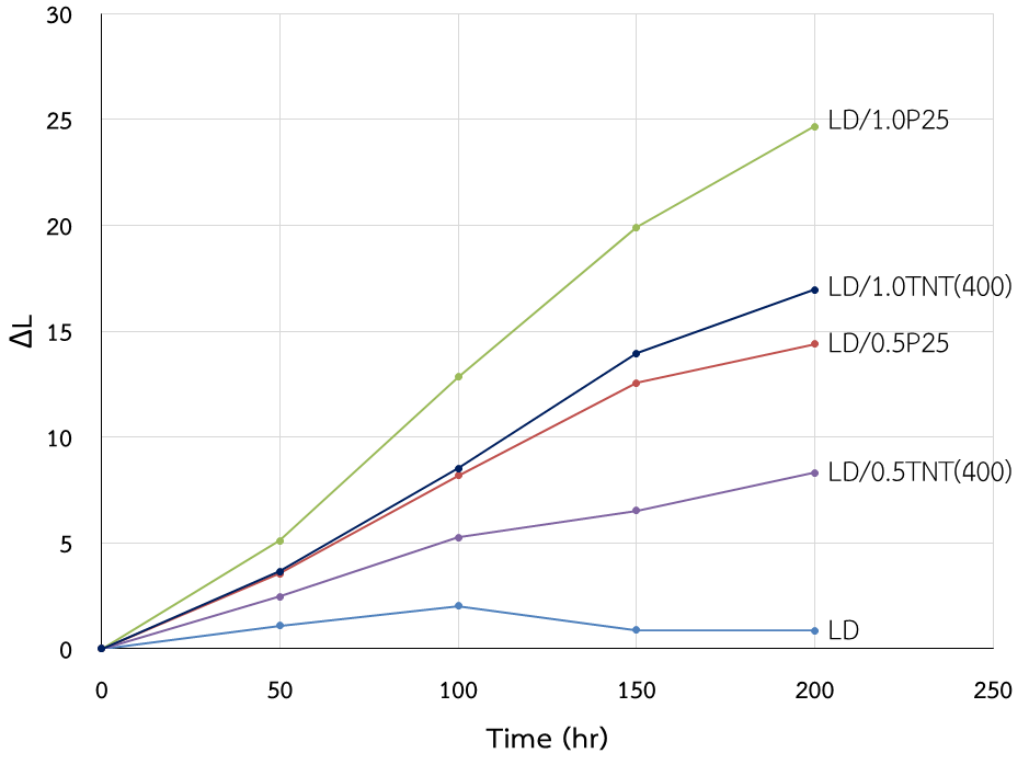

Figure 4.23 Lightness change (ΔL) LD, LD/0.5P25, LD/1.0P25, LD/0.5TNT(400) and LD/1.0TNT(400) at various UVA exposure times

Table 4.7 The opacity of LD, LD/0.5P25, LD/1.0P25, LD/0.5TNT(400) and LD/1.0TNT(400) at 0 and 200 hours of UVA irradiation

Sample	Film opacity (%)		
	0 hr	200 hrs	%Difference
LD	24.3	25.8	6.2
LD/0.5P25	41.2	54.0	31.1
LD/1.0P25	56.1	77.3	37.8
LD/0.5TNT(400)	31.8	40.1	26.1
LD/1.0TNT(400)	32.4	42.8	32.1

Opacity of photodegradable films was increased as catalyst loading from 0.5 to 1.0 phr. It is suggested that an increment of catalyst loading caused differences in light reflection and scattering in LDPE films. However, LDPE mixed with TNT had opacity lower than LDPE mixed with P25, even though catalyst loading of TNT(400) was higher than P25. Consequently, an accretion of P25 in LDPE film induced more light scattering in LDPE films, but TNT structure led to low refractive index of the films as explained in session 4.2.1.3 (Film opacity). Opacity of photodegradable films was enhanced after UVA exposure. So, a high value of opacity of photodegradable films was obtained. Film opacity had a similar trend, as compared to color and lightness change due to degradation of LDPE.

4.2.2.2 Mechanical properties of photodegradable films

Mechanical properties of photodegradable films before and after UVA exposures by Universal testing machine (UTM) are shown in Figures 4.24-4.26. It was found that LDPE film with and without catalyst before UVA exposures did not observe any significant change in tensile strength at break, %elongation at break and Young's modulus. It can be assumed that an addition small amount of catalyst loading from 0.5 to 1.0 phr in LDPE could not affect a significant differences in mechanical properties of photodegradable films. Tensile strength at break and Young's modulus of LDPE with catalyst at 0.5-1.0 phr after UVA exposures were increased. This is because LDPE was preferred crosslinked degradation. However, %elongation at break was reduced owing to chain scission and crosslinked degradation. Therefore, LDPE films with and without catalyst had possibility of both chain scission and crosslink phenomena.

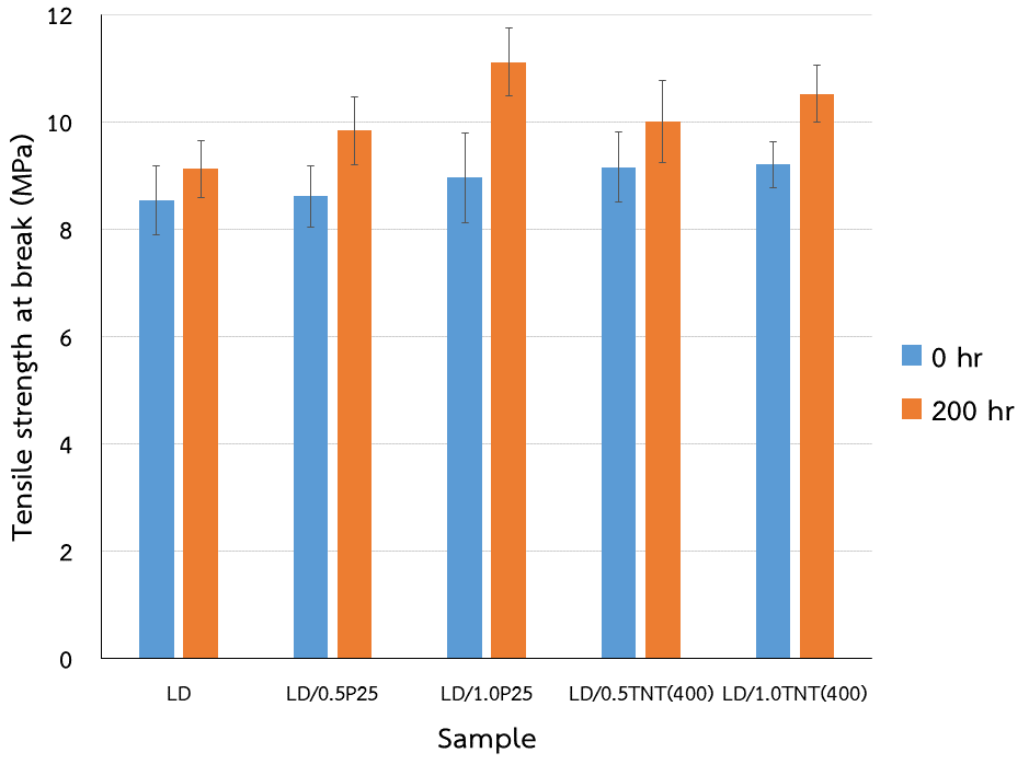

Figure 4.24 Tensile strength at break of LD, LD/0.5P25, LD/1.0P25, LD/0.5TNT(400) and LD/1.0TNT(400) at 0 and 200 hours

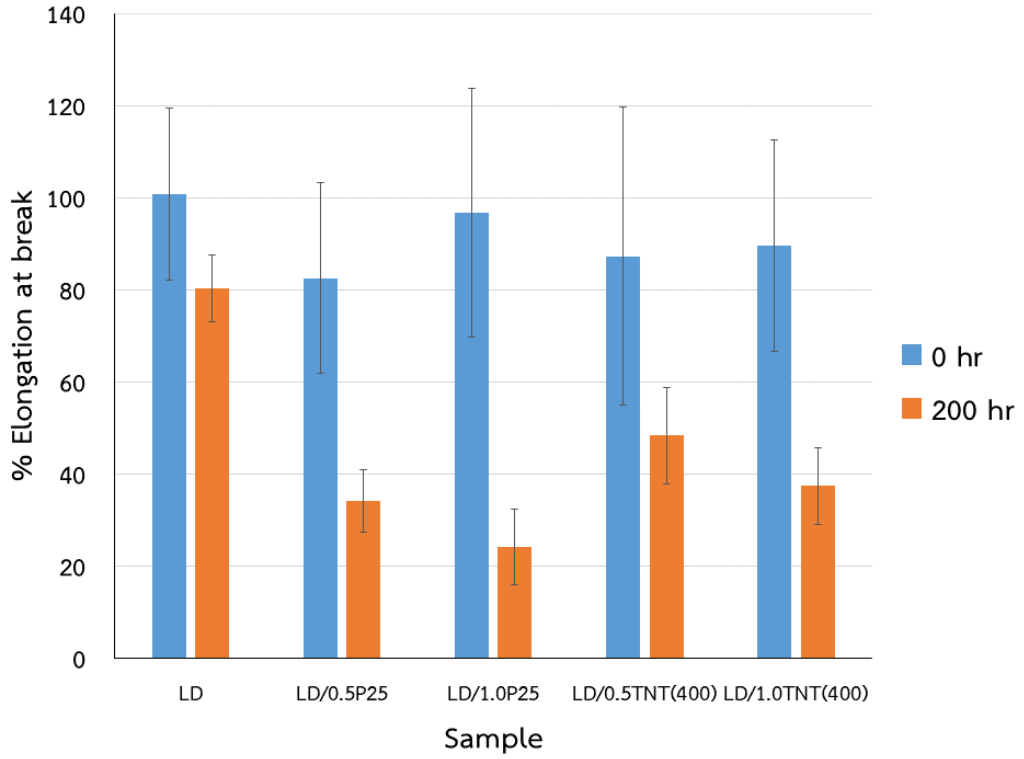

Figure 4.25 %Elongation at break of LD, LD/0.5P25, LD/1.0P25, LD/0.5TNT(400) and LD/1.0TNT(400) at 0 and 200 hours

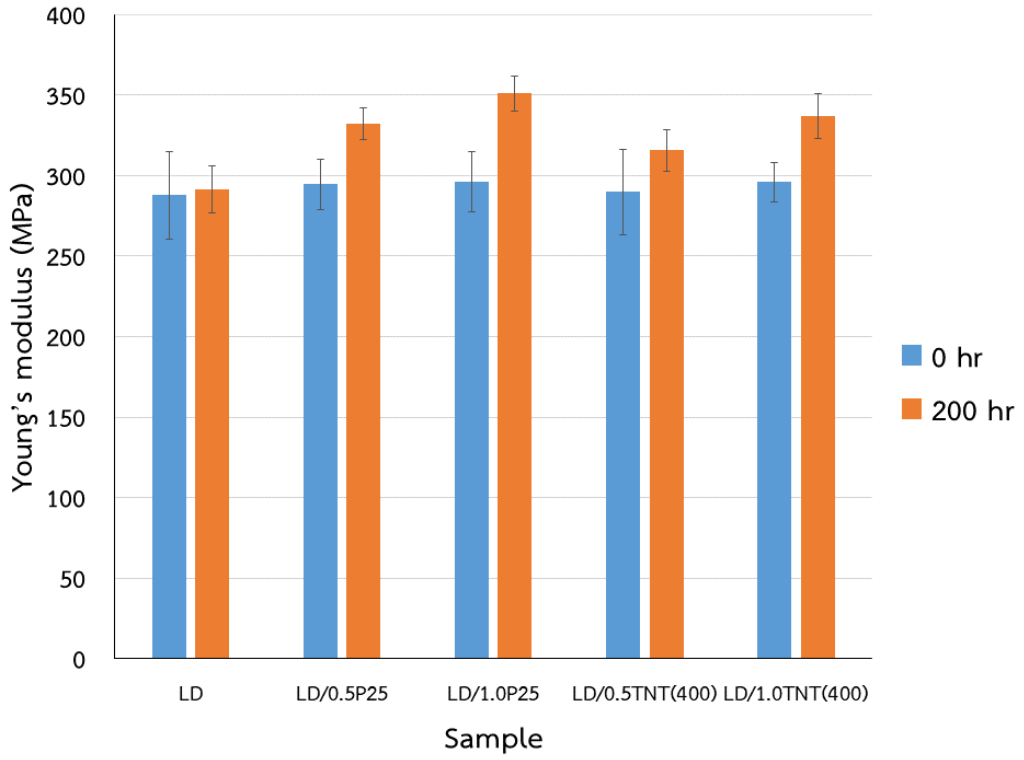

Figure 4.26 Young's modulus of LD, LD/0.5P25, LD/1.0P25, LD/0.5TNT(400) and LD/1.0TNT(400) at 0 and 200 hours

Chapter 5
Conclusion and Suggestions

5.1 Conclusion

This research was studied the effect of TiO_2 nanostructures including P25, titanate nanotube (TNT) and titanate nanosheet (TNS) on photodegrability of LDPE films. Compounds were prepared by mixing LDPE with P25, TNT or TNS/TBA^+. Finally, the effect of catalyst types and contents were investigated.

TNT was synthesized from P25 by hydrothermal synthesis. TNT was successfully prepared and clearly revealed that it had an open-end tube like structure. Lepidocrocite titanate, proton exchange of lepidocrocite titanate and TNS/TBA^+ was successfully obtained by a solid state synthesis, proton exchange and exfoliation process, respectively. Surface area of TNT(400) and TNS/TBA^+ were higher than P25 due to structure change from spherical to tube and sheet, respectively. Band gap energy of TNT(400) and TNS/TBA^+ were higher than P25 owing to the change of structural, crystal of catalyst and lower intensity of anatase phase. The photocatalytic activity of MO under UVA light irradiation, it was found that a trend of concentration of MO was reduced after UVA exposure related to higher intensity of anatase that could be attributed to a lower band gap energy.

Melting temperature and %crystallinity of photodegradable films mixed with and without catalyst had similar value. Therefore, addition of catalyst in LDPE did not interfere crystallinity of LDPE. Carbonyl index, %weight loss, color and lightness change of LDPE film mixed with and without catalyst after UVA exposures were increased. LDPE mixed with P25 or TNT(400) had poor dispersion and distribution in LDPE phase. This is because of differences in polarity between LDPE and P25 or TNT(400). On the other hand, LDPE mixed with TNS/TBA^+ had a better compatibility and dispersion than P25 or TNT(400) due to non-polarity of TBA^+ and LDPE. In addition, TNS/TBA^+ exhibited lower opacity than LDPE mixed with P25 and had a similar mechanical properties to LDPE. Tensile strength at break and Young's modulus of LDPE film mixed with and without catalyst after UVA exposures were not significant change. However, %elongation at break was decreased due to both possibilities of chain scission and crosslink phenomena.

Photodegradable films were improved at catalyst content from 0.5 to 1.0 phr, resulting in an increment of carbonyl index, %weight loss, color and lightness change. LDPE mixed with TNT(400) at loading of 1.0 phr had opacity lower than LDPE with P25 (0.5 phr). This is because TNT structure led to low refractive index of the films. Tensile strength at break and Young's modulus of photodegradable films were raised after UVA exposures owing to crosslinked degradation. However, %elongation at break was deteriorated due to possibility of both chain scission and crosslink phenomena.

5.2 Suggestions

1. LDPE incorporation with dispersing agents (i.e. stearic acid and octadecyl trichlorosilane) to improve dispersion of P25 or TNT.

2. Modification of catalyst with other substances to enhance the efficiency of degradation.

References

[1] Charles, E. and Carraher, Jr. 2012. **Introduction to Polymer Chemistry.** 3rd ed. Boca Raton : CRC/Taylor & Francis.

[2] The Essential Chemical Industry. 2013. **Degradable Plastics.** [Online]. Available : http://www.essentialChemicalindustry.org/polymers/degradable-plastics.html.

[3] Tohru, S. 2010. "Synthesis and Applications of Titanium Oxide Nanotubes." *Inorganic and Metallic Nanotubular Materials*. 117 : 17-32.

[4] Juan, C.C. Rafael, L. Juan, M.C. Fernando, C. Zbigniew, K. and Antonio, A.R. 2009. "Nanostructured Photocatalysts and Their Applications in the Photocatalytic Transformation of Lignocellulosic Biomass: An Overview." *Materials*. 2 : 2228-2258.

[5] ExcelPlas Australia, Centre for Design (RMIT) and Nolan ITU. 2004. **The Impacts of Degradable Plastic Bags in Australia.** Canberra : Victoria.

[6] Karli, J. and Tim, G. 2016. **LCA of Degradable Plastic Bags.** [Online]. Available : http://www.europeanplasticfilms.eu/docs/Jamesandgrant1.pdf.

[7] Francis, V. 2012. "Modification of Linear Low Density Polyethylene for Improved Photo and Biodegradation." Ph.D. Thesis, Cochin University of Science and Technology.

[8] Vasek, L. 2006. "Photodegradation of polyolefins." Bachelor Thesis, Faculty of Technology, Tomas Bata University in Zlín.

[9] Nagai, Y. Nakamura, D. Miyake, T. Ueno, H. Matsumoto, N. Kaji, A. and Ohishi, F. 2005. "Photodegradation Mechanisms in Poly(2,6-butylenenaphthalate- co-tetramethyleneglycol) (PBN–PTMG). I: Influence of the PTMG Content." *Polymer Degradation and Stability*. 88(2) : 251-255.

[10] Farnetti, E. Monte, D.R. and Kaspar, J. 2009. **Homogeneous and Heterogeneous Catalysis.** Trieste : EOLSS Publications.

[11] UC Davis ChemWiki. 2016. **An Introduction to Types of Catalysis.** [Online]. Available : http://chemwiki.ucdavis.edu/Core/Physical_Chemistry/Kinetics/Complex_Reactions/Catalysis/B._Catalysis/1._An_Introduction_to_Types_of_Catalysis.

[12] Zhao, X. Li, Z. Chen, Y. Shi, L. and Zhu, Y. 2006. "Solid-phase Photocatalytic Degradation of Polyethylene Plastic under UV and Solar Light Irradiation." *Journal of Molecular Catalysis A: Chemical*. 268 : 101–106.

[13] Mark, H.F. Bikales, N.M. Overberger, C.G. and Menges, G. 1986. **Encyclopedia of polymer science and engineering.** 2nd ed., vol. 4. New York : Wiley Interscience Publication.

[14] Bett, S. 2016. **What are Norrish Type-I and Type-II Reactions. Can Somebody Explain Them with Examples?.** [Online]. Available : https://www.quora.com/What-are-Norrish-type-I-and-type-II-reactions-Can-somebody-explain-them-with-examples.

[15] Kijima, T. 2010. "Synthesis and Applications of Titanium Oxide Nanotubes." *Inorganic and Metallic Nanotubular Materials*. 117 : 17–32.

[16] Carp, O. Huisman, C.L. and Reller, A. 2004. "Photoinduced Reactivity of Titanium Dioxide." *Progress in Solid State Chemistry*. 32 : 33–177.

[17] Thompson, R. 1995. **Industrial inorganic chemicals; production and uses.** Cambridge : The Royal Society of Chemistry.

[18] Zhang, H. and Banfield, J.F. 2000. "Understanding Polymorphic Phase Transformation Behavior during Growth of Nanocrystalline Aggregates: Insights from TiO_2." *The Journal of Physical Chemistry B*. 104 : 3481-3487.

[19] Ohtani, B. Prieto-Mahaney, O.O. Li D. and Abe, R. 2010. "What is Degussa (Evonik) P25? Crystalline Composition Analysis, Reconstruction from Isolated Pure Particles and Photocatalytic Activity test." *Journal of Photochemistry and Photobiology A: Chemistry*. 216(2-3) : 179-182.

[20] Evonik Industries. 2016. **AEROXIDE® TiO_2 P25.** [Online]. Available : http://corporate.evonik.com/en/products/search-products/Pages/product-details.aspx?pid=43469&pfcat=5070.

[21] Liu, N. Chen, X. Zhang, J. and Schwank J.W. 2014. “A Review on TiO_2-based Nanotubes Synthesized via Hydrothermal Method: Formation Mechanism, Structure Modification, and Photocatalytic Applications.” *Catalysis Today*. 225 : 34– 51.

[22] Bavykin, D.V. Friedrich, J.M. and Walsh, F.C. 2006. “Protonated Titanates and TiO_2 Nanostructured Materials: Synthesis, Properties, and Applications.” *Advanced Materials*. 18 : 2807–2824.

[23] Gong, D. Grimesa, C.A. Varghese, O.K. Hu, W. Singh, R.S. Chen, Z. and Dickey, E.C. 2001. “Titanium Oxide Nanotube Arrays Prepared by Anodic Oxidation.” *Journal of Materials Research*. 16 : 3331-3334.

[24] Gao, T. Fjellva, H. and Norby, P. 2009. “Defect Chemistry of a Zinc-Doped Lepidocrocite Titanate $Cs_xTi_{2-x/2}Zn_{x/2}O_4$ (x= 0.7) and its Protonic Form.” *Chemistry of Materials.* 21 : 3503–3513.

[25] Kaewmara, P. Maneerattanaamorn, W. and Netrungruang, W. 2014. “Preparation of Self-cleaning Glass by Coating with Lepidocrocite Titanate Nanosheets.” B.Sc. Special Project, King Mongkut's Institute of Technology Ladkrabang.

[26] Billmeyer, F.W. 1984. **Textbook of Polymer Science.** New York : John Willey & Sons.

[27] Kolev, M. 2016. **Polyethylene.** [Online]. Available : http://webhotel2.tut.fi/ projects/Caeds/tekstit/plastics/plastics_PE.pdf.

[28] Theerakarunwong, C. 2011. “Titanium Dioxide Photocatalysis” *Journal of Yala Rajabhat University.* 6(1) : 62-73.

[29] Chen, C. Wang, Z. Ruan, S. Zou, B. Zhao, M. and Wu, F. 2008. “Photocatalytic Degradation of C.I. Acid Orange 52 in The Presence of Zn-doped TiO_2 Prepared by a Stearic Acid Gel Method.” *Dyes and Pigments*. 77 : 204-209.

[30] Roy., P.K. Surekha, P. Rajagopal, C. Chatterjee, S.N. and Choudhary, V. 2007. “Studied on The Photo-oxidative Degradation of LDPE Films in The Presence of Oxidized Polyethylene.” Poly*mer Degradation and Stability*. 92 : 1151-1160.

[31] Kiatkittipong, K. Scott, J. and Amal, R. 2011. “Hydrothermally Synthesized Titanate Nanostructures: Impact of Heat Treatment on Particle Characteristics and Photocatalytic Properties.” *Applied Materials & Interfaces*. 3 : 3988–3996.

[32] Shibata, T. Sakai, N. Fukuda, K. Ebina, Y. and Sasaki, T. 2007. “Photocatalytic Properties of Titania Nanostructured Films Fabricated from Titania Nanosheets.” *Physical Chemistry Chemical Physics*. 9 : 2413-2420.

[33] Dong, X. Fu, J. and Xi, F. 2011. “Synthesis and Layer-by-Layer Self-assembly of Titania Nanosheets Controllably Doped with Binary Transition Metal Ions.” *Materials Research*. 26(10) : 1285-1291.

[34] Charassrisoonthorn, K. Simanta, P. and Sriloogwha, V. 2013. “Photocatalytic Degradation Film Prepared from LDPE/TiO_2 and LDPE/Zn-doped TiO_2.” B.Sc. Special Project (Industrial Chemistry), King Mongkut's Institute of Technology Ladkrabang.

[35] Rattanapaiboonkit, S. 2014. “Photodegradable Film Prepared from LDPE mixed with ZnO/TiO_2.” M.Sc. Thesis (Polymer Technology), King Mongkut's Institute of Technology Ladkrabang.

[36] Nada, A. Moustafa, Y. and Hamdy, A. 2014. “Improvement of Titanium Dioxide Nanotubes through Study Washing.” *British Journal of Environmental Sciences*. 2(4) : 29-40.

[37] Sasaki, T. Kooli, F. Iida, M. Michiue, Y. Takenouchi, S. Yajima, Y. Izumi, F. Chakoumakos, B.C. and Watanabe, M. 1998. “A Mixed Alkali Metal Titanate with the Lepidocrocite-like Layered Structure. Preparation, Crystal Structure, Protonic Form and Acid-Base Intercalation Properties.” *Chemistry of Materials*. 10 : 4123-4128.

[38] ColoRotate 2016. **Color theory.** [Online]. Available : http://learn.colorotate.org/color-models/#.V4fNDY9OKM8.

[39] ASTM Standard D882, 2012. " Standard Test Method for Tensile Properties of Thin Plastic Sheeting." ASTM International, West Conshohocken.

[40] Qamar M., Yoon C.R., Oh H.J., Lee N.H., Park K., Kim D.H., Lee K.S., Lee W.J. and Kim S.J. 2008. “Preparation and Photocatalytic Activity of Nanotubes Obtained from Titanium Dioxide.” *Catalysis Today*. 131 : 3–14.

[41] Fa W., Yang C., Gong C., Peng T. and Zan L. 2010. “Enhanced Photodegradation Efficiency of Polyethylene-TiO_2 Nanocomposite Film with Oxidized Polyethylene Wax.” *Journal of Applied Polymer Science*, 118(1) : 378-384.

[42] Masahiro M. and Hiromasa T. 2006. “Low-reflective and Super-Hydrophilic Properties of Titanate or Titania Nanotube Thin Films via Layer-by-Layer Assembly.” *Thin Solid Films*, 515 : 2091–2096.

Appendices

Appendix A
DR-UV-vis

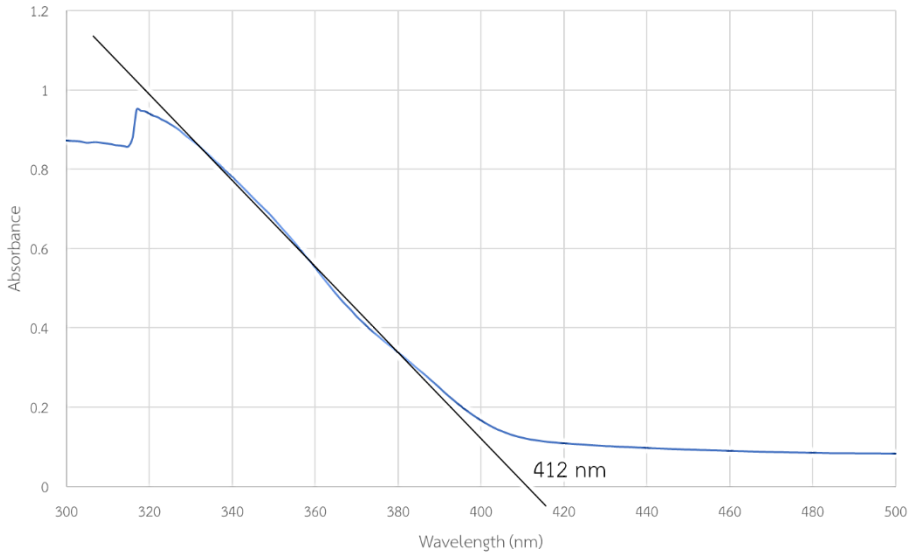

Figure A-1 Diffuse reflectance UV-visible spectroscopy (DR-UV-vis) of P25

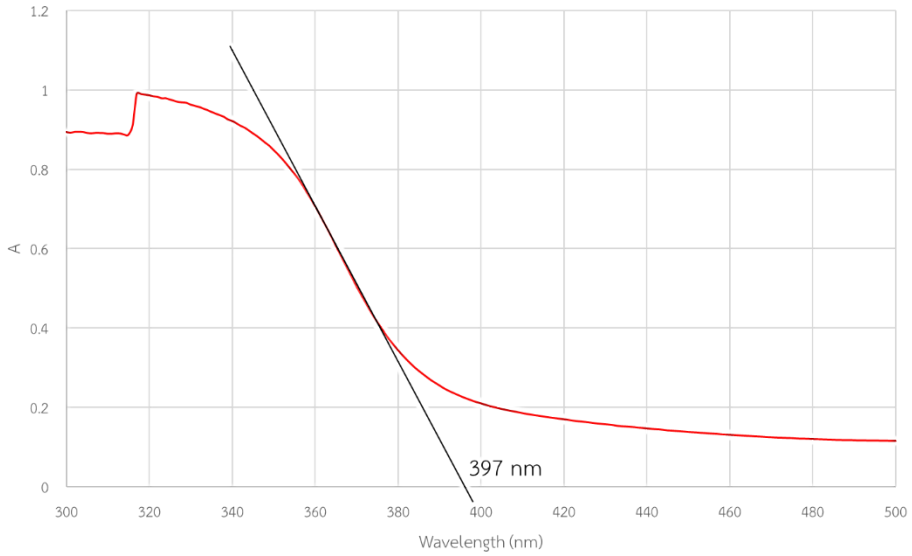

Figure A-2 Diffuse reflectance UV-visible spectroscopy (DR-UV-vis) of TNT(400)

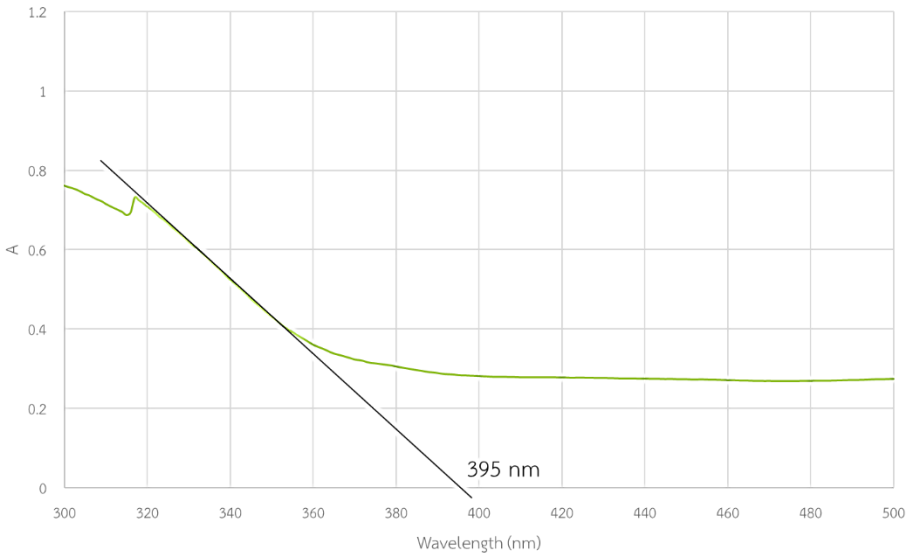

Figure A-3 Diffuse reflectance UV-visible spectroscopy (DR-UV-vis) of TNS/TBA^+

Appendix B
Methyl orange degradation

Table B-1 Photocatalytic oxidation of methyl orange (MO) under UVA irradiation from 0-30 minutes

Time (mins)	C/C_0						
	P25	TNT	TNT(300)	TNT(400)	TNT(500)	TNT(600)	TNS/TBA^+
0	1.00	1.00	1.00	1.00	1.00	1.00	1.00
10	0.67	0.99	0.87	0.79	0.82	0.84	0.99
20	0.52	0.98	0.79	0.67	0.72	0.77	0.99
30	0.34	0.95	0.72	0.45	0.54	0.64	0.98

Appendix C
DSC

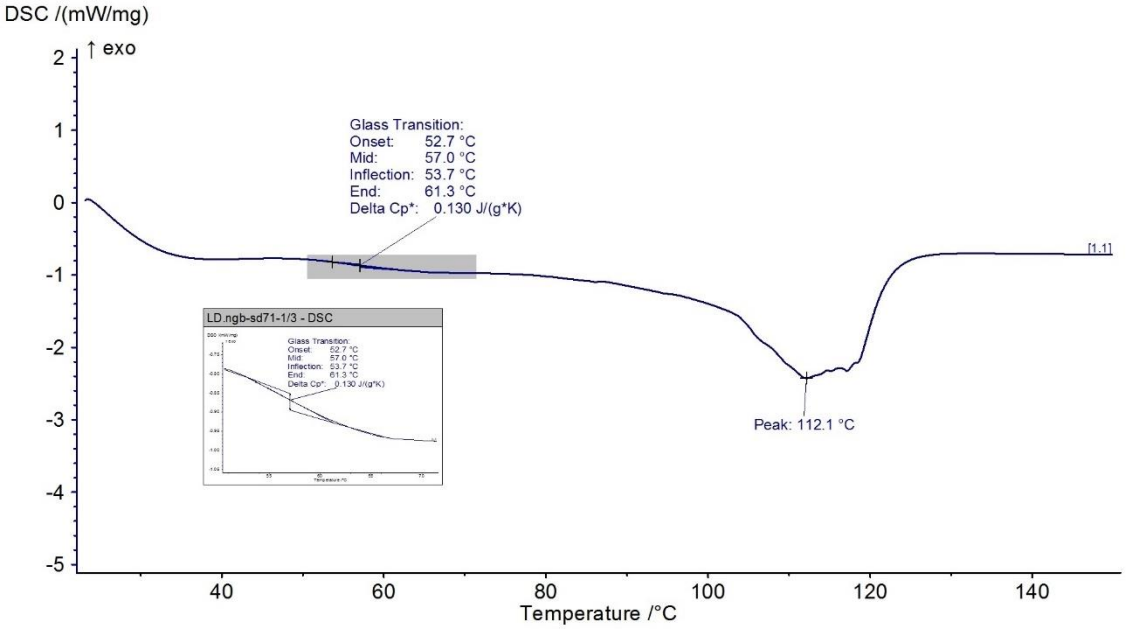

Figure C-1 DSC thermogram of LD

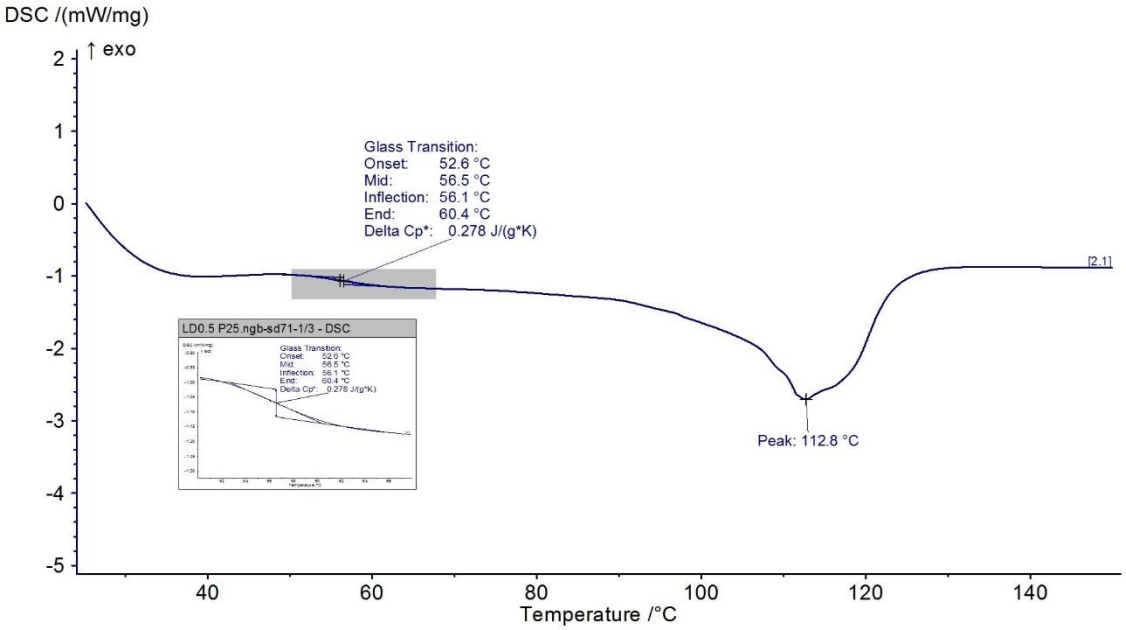

Figure C-2 DSC thermogram of LD/0.5P25

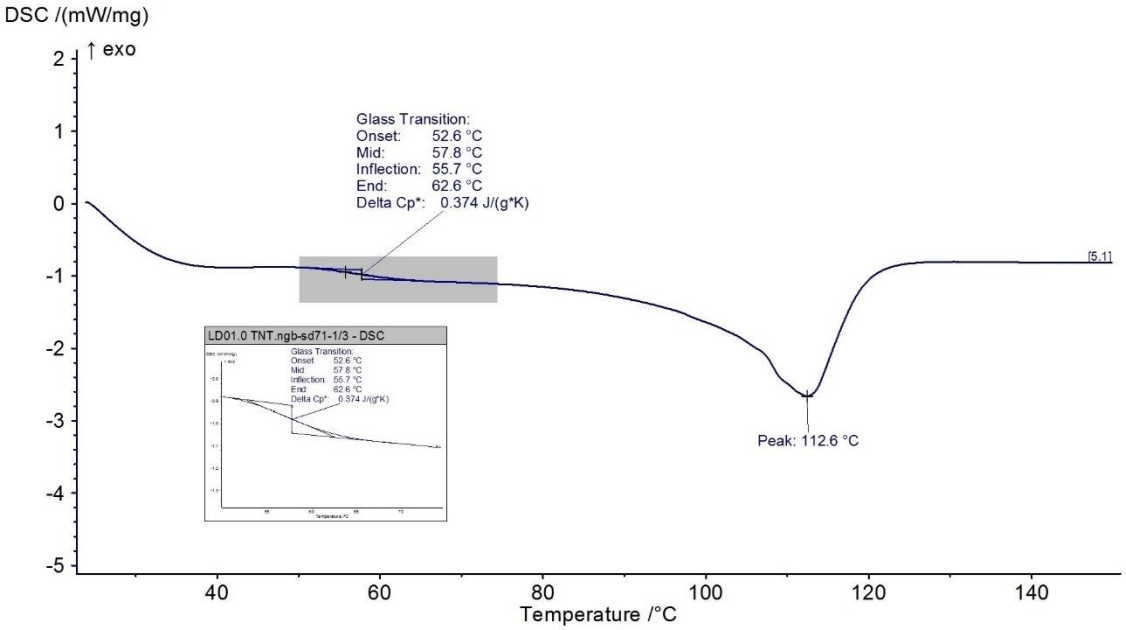

Figure C-3 DSC thermogram of LD/0.5TNT(400)

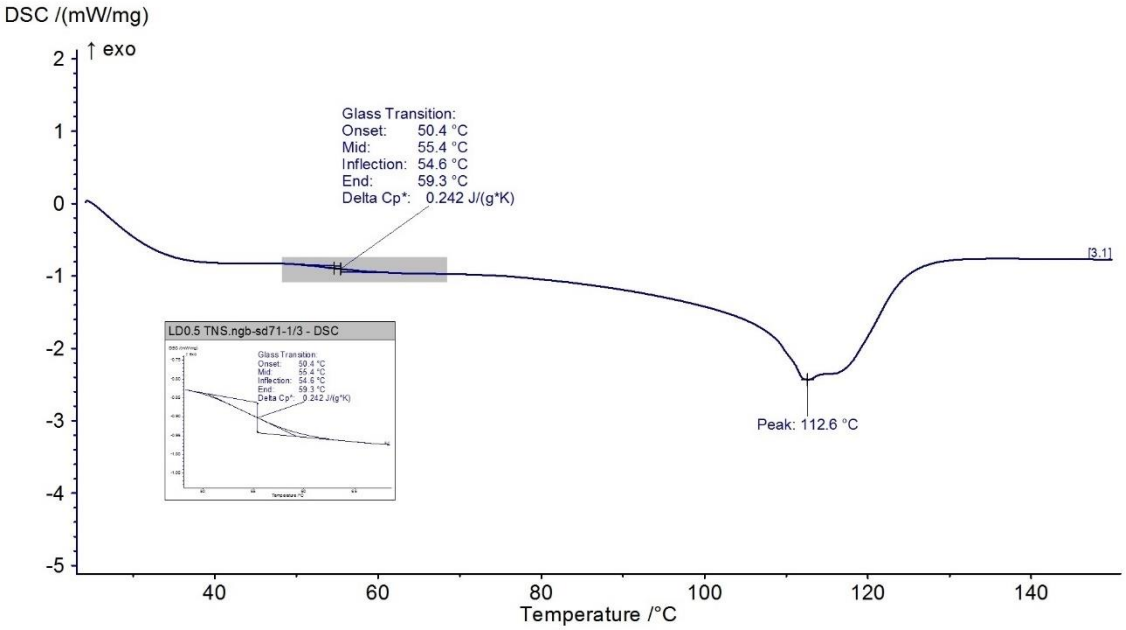

Figure C-4 DSC thermogram of LD/2.0TNS/TBA^+

Appendix D
Carbonyl index (C.I.)

Table D-1 Carbonyl index (C.I.) of photodegradable films at various UVA exposure times

Time (hrs)	Carbonyl index (C.I.)					
	LD	LD/ 0.5P25	LD/ 1.0P25	LD/ 0.5TNT(400)	LD/ 1.0TNT(400)	LD/ 2.0TNS/TBA^+
0	0.0000	0.0000	0.0000	0.0000	0.0000	0.0000
50	0.0027	0.0117	0.0228	0.0064	0.0151	0.0035
100	0.0121	0.0344	0.0641	0.0196	0.0410	0.0136
150	0.0199	0.0543	0.1045	0.0309	0.0630	0.0224
200	0.0226	0.0693	0.1286	0.0373	0.0800	0.0267

Appendix E
%Weight loss

Table E-1 %Weight loss of photodegradable films at various UVA exposure times

Time (hrs)	%Weight loss					
	LD	LD/ 0.5P25	LD/ 1.0P25	LD/ 0.5TNT(400)	LD/ 1.0TNT(400)	LD/ 2.0TNS/TBA^+
0	0	0	0	0	0	0
50	0.0679	1.0186	1.4517	0.7976	1.0754	0.0912
100	0.1083	1.7473	3.1279	1.2203	1.9254	0.1874
150	0.1491	2.4599	4.8284	1.5501	2.6256	0.2535
200	0.1762	3.3262	7.1885	1.6681	3.4927	0.2839

Appendix F
Color change (ΔE)

Table F-1 Color change of photodegradable films at various UVA exposure times

Sample	Time (hrs)	L*	a*	b*	ΔE
LD	0	24.44	-1.25	-2.99	0
	50	28.53	-0.62	-3.97	1.79
	100	29.74	-0.71	-3.80	1.84
	150	28.34	-1.35	-2.94	1.95
	200	28.31	-0.99	-3.45	1.98
LD/0.5P25	0	40.320	-1.48	-9.88	0
	50	43.87	-0.93	-9.53	2.21
	100	48.5	-0.53	-7.98	3.27
	150	52.89	-1.34	-7.05	3.93
	200	54.73	-0.57	-2.57	4.19
LD/1.0P25	0	55.95	-3.17	-9.86	0
	50	61.05	-2.15	-7.70	2.78
	100	68.79	-0.78	-3.92	4.58
	150	75.85	-1.25	-1.26	5.51
	200	80.61	-1.02	-0.76	5.82
LD/0.5TNT(400)	0	33.03	-1.14	-1.97	0
	50	35.49	-0.62	-3.69	2.17
	100	38.28	-0.32	-3.41	2.73
	150	39.55	-1.24	-2.4	3.13
	200	41.34	0.55	-2.75	3.31
LD/1.0TNT(400)	0	34.59	-0.89	-0.4	0
	50	38.26	-1.13	-2.05	2.35
	100	43.12	-0.19	-3.09	3.44
	150	48.55	-0.76	-2.35	3.99
	200	51.55	-0.32	-2.39	4.34

Table F-1 (continued) Color change of photodegradable films at various UVA exposure times

Sample	Time (hrs)	L*	a*	b*	ΔE
LD/2.0TNS/TBA^{+}	0	31.27	-1.18	-1.04	0
	50	32.18	-1.31	-1.64	1.10
	100	32.57	-0.93	-1.65	1.45
	150	32.92	-0.74	-1.78	1.86
	200	33.21	-0.68	-1.81	2.17

Appendix G
Mechanical properties

Table G-1 Mechanical properties of photodegradable films at 0 and 200 hours

Sample	Tensile strength at break (MPa)	%Elongation at break	Young's modulus (MPa)
Before UVA exposure			
LD	8.5 ± 0.64	101 ± 18.63	288 ± 27.25
LD/0.5P25	8.6 ± 0.57	83 ± 20.78	294 ± 15.72
LD/1.0P25	9.0 ± 0.83	97 ± 26.97	296 ± 18.64
LD/0.5TNT(400)	9.1 ± 0.65	87 ± 32.38	290 ± 26.39
LD/1.0TNT(400)	9.2 ± 0.43	90 ± 22.92	296 ± 12.04
LD/2.0TNS/TBA^+	9.8 ± 0.52	106 ± 21.46	300 ± 19.15
After UVA exposure for 200 hours			
LD	9.1 ± 0.53	80 ± 7.27	291 ± 14.65
LD/0.5P25	9.8 ± 0.63	34 ± 6.81	332 ± 9.87
LD/1.0P25	11.1 ± 0.63	24 ± 8.25	351 ± 10.84
LD/0.5TNT(400)	10.0 ± 0.76	48 ± 10.36	316 ± 12.97
LD/1.0TNT(400)	10.5 ± 0.53	37 ± 8.35	337 ± 14.02
LD/2.0TNS/TBA^+	10.4 ± 0.44	81 ± 7.69	307 ± 10.91

Author Biography

Name Mr. Pratya Kunjit

Date of Birth 12 March 1992

Address Ramintra, Kannayao, Bangkok, Thailand

Education 2014 Bachelor of Science in Industrial Chemistry GPA 3.45
King Mongkut's Institute of Technology Ladkrabang

Scholarship Scholarship to Conference at International Polymer Conference of Thailand (PCT-6)

Academic Publication(s)

Pratya Kunjit, Tawan Sooknoi, Tosapol Maluangnont, Suparat Rukchonlatee and Chonlada Ritvirulh, "Photodegradable film prepared from LDPE/TiO_2 nanotube", *The proceedings of The International Polymer Conference of Thailand* (PCT-6), June 30-July 1, Bangkok, Thailand, pp. 452-456, 2016.